Volcanic History of the Tempe Volcanic Province

by

Leon Manfredi

A Thesis Presented in Partial Fulfillment
of the Requirements for the Degree
Master of Science

Approved August 2012 by the
Graduate Supervisory Committee:

David Williams, Co-Chair
Amanda Clarke, Co-Chair
Stephen Reynolds

ARIZONA STATE UNIVERSITY

December 2012

ABSTRACT

Tempe Terra, Mars, has a complex history marked by volcanism and tectonism. Investigation results presented here build on previous work to better determine the volcanic history of the Tempe volcanic province by identifying and mapping previously undetected vents, characterizing all vents, identifying spatial and temporal trends in eruptive styles, comparing vent density to similar provinces such as the Snake River Plains of Idaho and Syria Planum and determining absolute age relationships among the volcanic features.

Crater size-frequency distribution model ages of 120 Ma to 2.4 Ga indicate the province has been active for over half of the planet's history. During that time, age decreases from southwest to northeast, a trend that parallels the dominant orientation of faulting in the region, providing further evidence that volcanic activity in the region is tectonically controlled (or the tectonics is magmatically controlled). Morphological variation with age hints at an evolving magma source (increasing viscosity) or changing eruption conditions (decreasing eruption rate or eruption through thicker lithosphere).

DEDICATION

This thesis is dedicated to my loving wife, Julia. Without her I would still be a computer programmer at a job I did not like. She gave me the courage to go back to school and pursue my dreams. Her support for the last six years has allowed me to be the student I am. Finishing this will allow me to keep your appreciation bucket ever full.

ACKNOWLEDGMENTS

I would first like to thank the late Dr. Ronald Greeley for giving me the opportunity to study under him. His guidance as a teacher, advisor, and mentor are sorely missed. I would like to thank my committee members, Dr. Amanda Clarke, Dr. David Williams, and Dr. Steve Reynolds for their time and support. I would also like to thank all the professors at SESE for sharing their wisdom. Thanks to Dr. Wendy Taylor and Meg Hufford for their help and exposure to Education and Public Outreach. Thank you Sheri Klug Boonstra for the flexibility to finish my thesis while working. Finally, thanks to Charles Bradbury, Stephanie Holiday, Rebekah Keinenburger, Melissa Bunte, Devin Waller, Amy Zink, and Dan Ball for their help along the way.

TABLE OF CONTENTS

CHAPTER Page

LIST OF TABLES

LIST OF FIGURES

Chapter 1

INTRODUCTION

Objective

The objective of this research is to investigate volcanism in the Tempe volcanic province (TVP), Mars, in order to identify previously undetected vents, to characterize all vents based on morphology, to identify spatial and temporal and volcanic trends, to determine the relationship between volcanism and structure, and to use morphology as a proxy for eruption conditions and magma characteristics. This area was identified by Hodges (1980) and Plescia (1980). Understanding the volcanic history of the TVP is important for understanding how a field of low shields evolves, how volcanism is related to the local and regional tectonic setting, and how the TVP is related to or compares to volcanism in other volcanic provinces. This information may help us understand how fields of low shields develop on Earth and on other planetary bodies that do not currently have plate tectonics (e.g., Mars, Moon, Venus).

Background

Tempe Terra (Figure 1) is a plateau approximately 1800 km across and composes the northwestern extent of the Tharsis rise along the dichotomy boundary of Mars. Tempe Terra can be divided into two surfaces consisting of older, Noachian, heavily cratered and fractured highland material embayed by younger, Hesperian and Amazonian, volcanic material (Wise, 1979; Moore, 2001). Graben trending predominantly southwest to northeast transect both

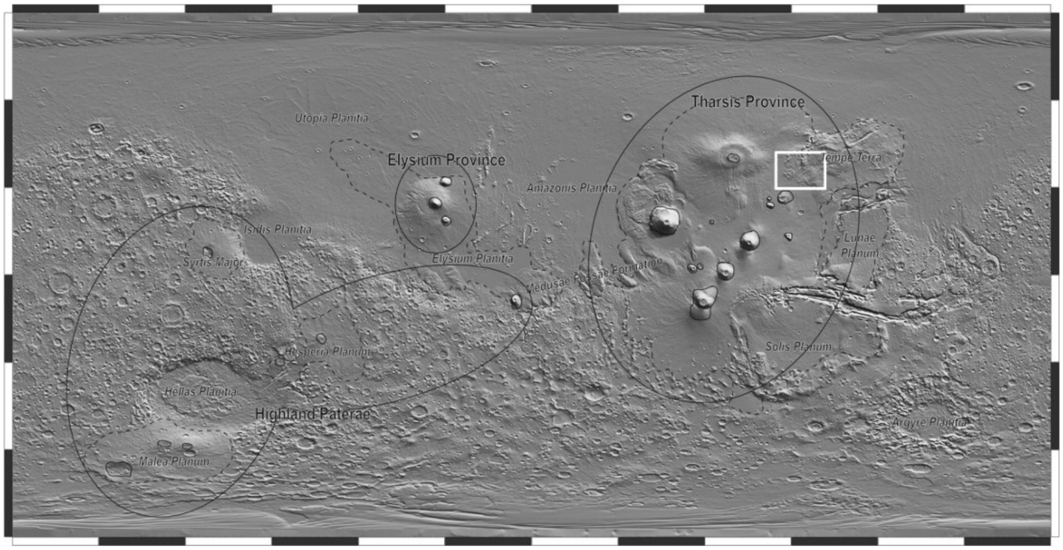

Figure 1. Volcanic provinces of Mars. Modified from Werner (2009). Solid lines outline central vent edifices, white box identifies the TVP. Background is Mars Orbiter Laser Altimeter (MOLA) shaded relief.

surfaces and have been hypothesized to control volcanism in the region (Hodges, 1980; Plescia, 1981**;** Scott, 1982).

Mars was imaged by several spacecraft in the Mariner program; Mariner 4 flyby (1965), Mariner 6 and 7 flybys (1969), and Mariner 9 orbiter (1971-72). Images from flybys of Mariner 4 (average resolution ~ 3 km/pix), 6 and 7 (resolutions as high as ~ 300 m/pix), which covered only a small percentage of the martian surface, showed a cratered surface similar to the Moon. It was not until Mariner 9 entered orbit that more of the surface could be imaged (resolutions between 1 km/pix to 100 m/pix). Geologic mapping based on Mariner 9 data identified Amazonian aged smooth plains material (Aps) interpreted to be aeolian and volcanic deposits in the TVP, however no vents were identified (Scott & Carr, 1978).

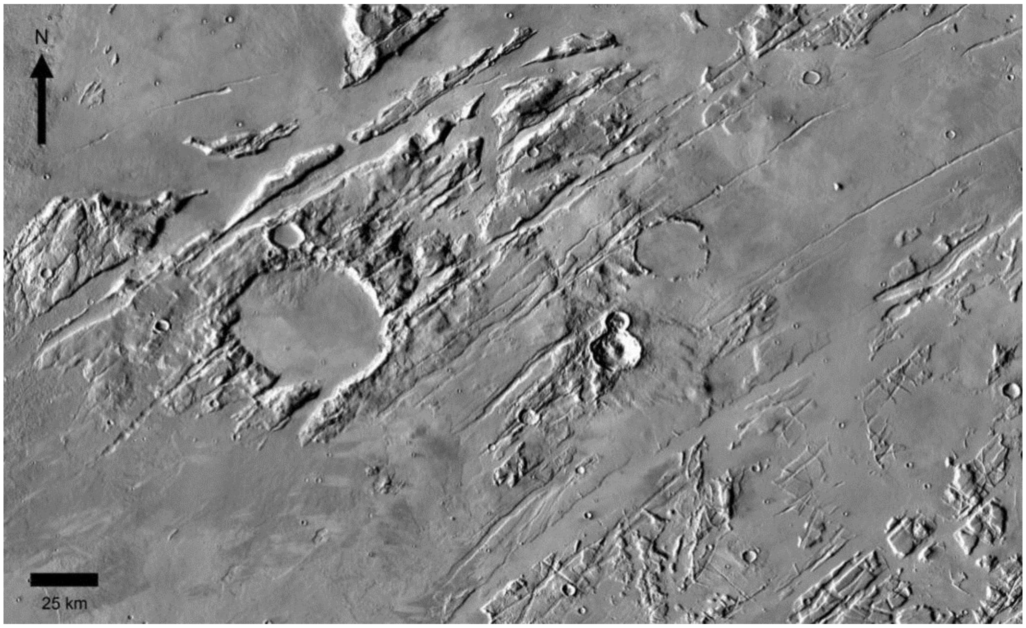

Figure 2. Graben in the TVP. The dominant orientation is SW to NE but several younger graben with a N to S orientation are present. Background is a mosaic of THEMIS day IR images.

Images returned from the Viking orbiters (~200 m/pix) in the mid-1970's enabled identification of smaller features not resolvable in Mariner 9 images. These features include low shield volcanoes with diameters less than 10s of kilometers (Greeley, 1982), and fissure vents. Other workers also identified these features in the TVP from Viking images (Hodges, 1979,1980**;** Hodges & Moore, 1994). More detailed analysis of volcanism in the TVP was done by Plescia (1981), who grouped the features by styles of volcanism: flood basalts, plains volcanism, scattered fissure vents, and steeper conical features with summit craters. Due to the low relief of many of the features and the resolution of the Viking images, only a handful of vents were identified.

After Viking, new orbital data was not available until the Mars Global Surveyor (MGS) entered orbit in 1997. Onboard were two instruments, the Mars

Orbiter Camera (MOC) (Malin et al., 1998) and Mars Orbiter Laser Altimeter (MOLA) (Zuber et al., 1992; Smith et al., 2001), that would further help identify and classify volcanic features in the TVP. The MOC narrow angle camera (typically 1.5 to 12 m/pix) revealed radial textures thought to be related to lava flows on some volcanic features (Malin & Edgett, 2001). MOLA data (~ 1 km/pix) provided elevation information used to generate digital elevation models (DEMs). These data were then used to identify volcanic features previously undetected due to very shallow slopes, and to compare edifice morphometry of vents in the TVP to other martian vents and terrestrial vents (Head, 2001; Wong et al., 2001; Hauber et al., 2009).

The turn of the century saw a dramatic increase in the number of spacecraft in orbit around Mars beginning with Mars Odyssey in 2001, Mars Express (MEX) in 2003, and Mars Reconnaissance Orbiter (MRO) in 2006. Each mission brought new instruments to bear on the surface of Mars to address unanswered questions.

The Thermal Emission Imaging System (THEMIS) camera on Odyssey has returned images in both the visible (VIS) and IR spectrum at resolutions of 18 m/pix for visible images and 100 m/pix for IR images (Christensen et al., 2004). While THEMIS VIS images offer lower resolution than MOC images, they have greater spatial coverage. THEMIS VIS images have been used to determine that many previously identified shields are actually the summits of much larger shields that have been embayed by younger lava flows and have morphologies linked to petrologic variations due to percent volume phenocrysts and gas/vesicle content

(Sakimoto et al., 2003). THEMIS images were also used to identify shields for morphologic studies, while a petrologic model was applied to suggest that the low shields are the result of multiple injections of primary magma through a regional sill network (Hughes et al., 2008). Further use of THEMIS images identified shields for area and volume comparisons to terrestrial shields (Hauber et al., 2009).

The High Resolution Stereo Camera (HRSC) (Neukum and Jaumann, 2004) camera on the MEX spacecraft has imaged the TVP at resolutions of approximately 12 m/pix. These images have been used to study the surface in the visible spectrum as well as with DEMs (10-40 m/pix) produced from stereo images. These data have been used to map volcanic features and compare topography and morphology of shields in TVP to Earth analogues (Hauber et al., 2009; Baratoux et al., 2009) and to compare low shields in Syria Planum (Baptista et al., 2008) to those in TVP. This work confirmed the findings reported by Plescia (1981), that the low shields of the SRP, the TVP, and Syria Planum have similar morphologies.

Two instruments on MRO, the Context Camera (CTX) (Malin et al., 2007) and High Resolution Imaging Science Experiment (HiRISE) (*McEwen et al.*, 2007), have contributed to the exploration of the TVP. Large swath widths (~ 30 km) and resolutions ~ 5-6 m/pix have enabled the CTX camera to image much of the TVP, and these images enable the acquisition of absolute model ages of volcanic surfaces using impact crater size-frequency distributions (CSFD) (Hauber et al., 2011). While HiRISE images have extremely high resolution (~30 cm/pix), their limited spatial coverage (swath widths of ~ 6 km) result in only portions of a shield to be imaged. Hauber et al. (2011) used HiRISE images to count craters on lava flows and shields down to about 20 m in diameter in the TVP to determine CSFD absolute model ages.

Volcanism on Mars

Hodges and Moore (1994) cataloged the variety of volcanic features seen on Mars using Viking data and identified shields as small as a few tens of km in diameter. Since their work, most of Mars has been imaged at resolutions of 100 m/pix (THEMIS Day IR Global Mosaic) and more than 50% has been imaged at 5-6 m/pix with the CTX camera, enabling the identification of even smaller volcanic features (Lanz and Saric, 2009; Hauber et al., 2011; Ryan and Christensen, 2012). Many lines of evidence, presented below, suggest nearly all forms of volcanism are mafic in composition. Morphologically, martian shields are similar to those on Earth (Greeley and Spudis, 1981; Bleacher et al., 2007a,b; Hauber et al., 2009). Mineralogy of the martian surface has been investigated from orbit (Bandfield, 2002) as well as from in situ measurements (Baird et al., 1976; Ruff et al., 2006), and martian meteorites (McSween, 1984, 1994), and indicate volcanic rocks are basaltic. Felsic volcanic features (i.e., composite cones, stratovolcanoes, granite) have yet to be identified (Francis and Wood, 1982), an aspect that distinguishes the martian crust from that of Earth. Like basaltic volcanism on Earth, volcanism on Mars can be grouped into three styles of volcanism: flood, point source, and plains.

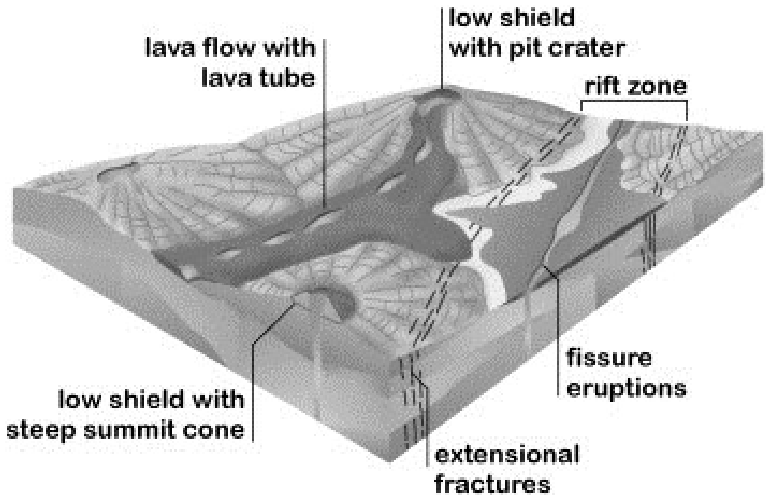

Figure 3. Idealized representation of the features seen in the Snake River Plain, referred to as Plains-style volcanism. These features are analogous to features seen in the TVP. Figure from Hauber et al. (2009).

Styles of Volcanism.

Flood. Flood volcanism is thought to be generated from fissures with high rates of effusion and large volumes of lava, producing large volcanic plains (Walker, 1971; Greeley, 1976; Self et al., 1997). Examples on Earth include the Columbia River Basalts, Deccan Traps, and Siberian Traps (White and McKenzie, 1989; Campbell and Griffiths, 1990). Much of the martian surface, more than 60%, is covered in flood basalts (Greeley and Spudis, 1981) and represents the oldest style of volcanism seen on the planet (Greeley and Spudis, 1981; Werner, 2009). These units are classified as volcanic units based on the following criteria: lava flow fronts, embayment relationships, and the presence of wrinkle ridges. Wrinkle ridges alone are not diagnostic of volcanic material because they are also found in sedimentary units on Earth (Plescia and Golombek, 1986) but can be volcanic in origin as they are observed on continental flood basalts on Earth and on plains units interpreted to be volcanic in origin on the Moon, Mars, and Mercury (Watters, 1988).

Point source. Unlike flood basalts, which most likely erupt along the length of a fissure, point source volcanism originates from a central source. These volcanoes can be produced during a single eruption (monogenetic) or may be active for an extended period of time with periods of quiescence between eruptions (polygenetic). Based on morphology, the large (100's of kilometers in diameter) volcanoes on Mars appear to be shield volcanoes. These volcanoes have very shallow flank slopes suggesting the eruption of lavas with very low viscosities. It has been suggested that one shield, Hecates Tholus, shows signs of explosive activity as indicated by the surface texture and a paucity of impact craters on the western flank, attributed to airfall deposits (Mouginis-Mark, 1982). Other volcanic edifices associated with explosive eruptions (e.g., Tyrrhenus Mons, Hadriacus Mons) are located in the cratered highlands of the southern hemisphere. Greeley and Spudis (1981) termed these volcanoes "ash shields" due to their highly channelized flanks, suggestive of a low erosion resistant surface, and have been proposed to have formed by a combination of effusive and explosive events.

Plains style**.** Intermediate between flood volcanism and Hawaiian style shield volcanism is plains volcanism. This term was defined by Greeley (1982) while studying volcanoes in the eastern Snake River Plain. This style is characterized by low shields (flank slopes often less than 1 degree) that often coalesce into shield clusters, fissure-fed flows, vents aligned along rift zones, and multiple lava tube and channel fed flows, while many of these features have been attributed to high effusion rates (Figure 3). This style of volcanism is inferred to occur on and proximal to the larger (100's km in diameter) shields on Mars, such as the Tharsis shields and Elysium shields (Plescia, 1981; Baptista et al., 2008; Hauber, 2009; Bleacher et al., 2009).

Volcanic provinces. Volcanism on Mars is widespread but it is concentrated primarily in three provinces. Two of the provinces, Tharsis and Elysium are topographically and morphologically distinct from the third, circum-Hellas.

Tharsis Province. Located near the equator, Tharsis is the largest volcanic province on Mars. It is dominated by Olympus Mons, Alba Patera, and the three Tharsis Montes named Ascraeus Mons, Pavonis Mons, and Arsia Mons. Olympus Mons and the Tharsis Montes all share many characteristics with Hawaiian basaltic shield volcanoes (Carr, 1973, Bleacher and Greeley, 2008). While Olympus Mons has the distinction of being the tallest volcano in the solar system with a height of ~22 km, Alba Patera covers the most area with a diameter ~1000 km and has no known analog. Tharsis has other smaller shields as well as volcanoes classified as tholi or domes. The domes have steeper flank slopes than the shields and have been embayed by younger lavas that hide their true extent. Located within the Tharsis province are several fields of low shield volcanoes (e.g., Syria Planum, and TVP).

Based on CSFD model ages for surfaces in calderas, flanks, and the surrounding volcanic plains, the Tharsis region has seen activity from 4.0 Ga to

64 Ma (Werner, 2009). Newer CSFD work indicates that the province may have seen activity as recently as 52 Ma (Hauber et al., 2011). No surface on Earth has seen volcanic activity for such a long continuous period of time. The long-lived activity has been attributed to mantle upwelling, combined with a lack of plate tectonics (Steinberger et al., 2010). The morphological similarity between the shields of Tharsis and the Hawaiian shields (Bleacher et al., 2007a,b), which have been attributed to volcanism due to mantle upwelling, offers further evidence to support a mantle upwelling origin for the Tharsis province (Carr, 1973).

Upwelling is thought to be responsible for the updoming of Tharsis seen in topographic data and to have resulted in the formation of a fracture system that is roughly radial to Tharsis (Carr, 1974). Updoming appears to have taken place contemporaneously with the formation of the shields as the location of the shields appears to be controlled by the fractures.

Elysium Province. Located in the northern hemisphere, just north of the crustal dichotomy in the northern lowland plains, is the second largest volcanic province, dominated by three large volcanoes: Elysium Mons, Hecates Tholus, and Albor Tholus. Unlike the shields of Tharsis, the three largest volcanoes in Elysium are classified as domes due to their steeper flank slopes, between 1 and 10 degrees. Further to the south, on the dichotomy boundary, is the fourth large volcano in Elysium, Apollinaris Patera. Unlike the other large volcanoes that are grouped to the north, Apollinaris Patera is thought to be a composite volcano made of interbedded lava and pyroclastic material (Robinson et al., 1993). The

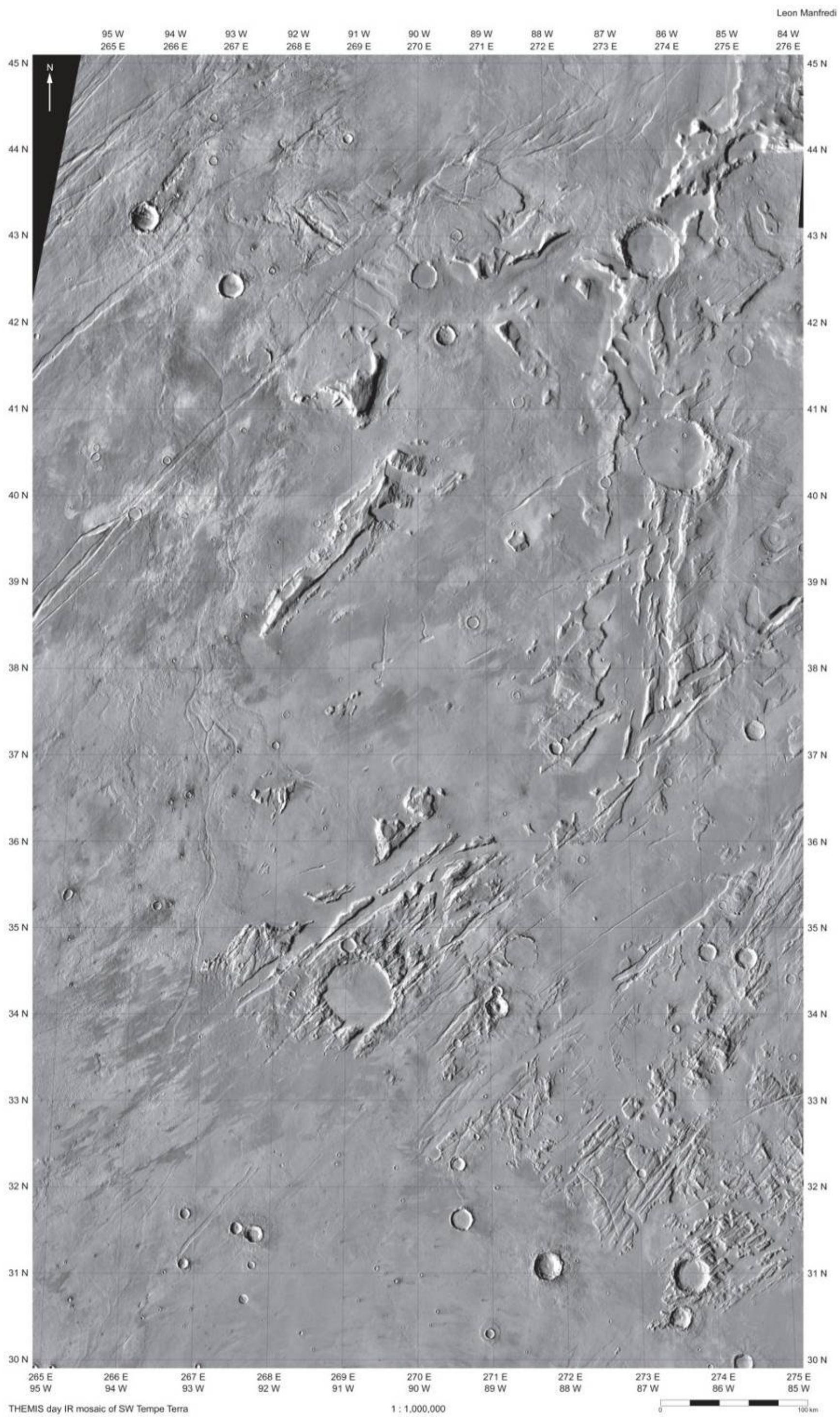

Figure 4. Base map made from mosaicking THEMIS day IR images of the TVP.

Elysium province also hosts a field of plains style, low shield volcanoes (Sakimoto, 2008).

Werner (2009) found a CSFD modeled age of approximately 3.8 Ga to 50 Ma for the region indicating that it is nearly as long lived as Tharsis. More recent work by Platz and Michael (2011), which dates 190 lava flows found similar ages ranging from 3.9 Ga to 60 Ma. Like Tharsis, the Elysium province sits on a topographic high or dome and may be due to mantle upwelling (Steinberger et al., 2010). Like Apollinaris Patera, Hecates Tholus may have undergone a period of explosive eruptions, as discussed above; crater isofrequency mapping suggests a mantling of a discrete, air-fall deposit on the western flank of Hecates Tholus (Mouginis-Mark et al., 1982).

Circum-Hellas Province (CHVP). In stark contrast to the topographically distinct volcanic provinces of Tharsis and Elysium, the CHVP has low relief compared to the surrounding terrain. This province is in the southern hemisphere and as the name implies, is situated around the Hellas Basin. The six volcanoes in the province fall into two styles of volcanism: shields (Tyrrhenus and Hadriacus Mons, and Amphitrites Patera) and caldera-like depressions surrounded by ridged plains (Peneus, Malea, and Pityusa Patera), which have been termed ash shields.

CSFD model ages of associated surfaces give ages between 3.6 to 3.9 Ga indicating that volcanism was active in this province contemporaneously with the other provinces but for some reason, activity ceased fairly quickly (Williams et al., 2009).

Not only is this province morphologically and temporally distinct from the other provinces, there is no sign of mantle upwelling under the CHVP (Steinberger et al., 2010). However, positive gravity anomalies have been detected under the shield-like volcanoes but not the ash shields (Williams et al., 2009). These data taken together suggest a difference in their formation mechanism, styles of eruption, and possibly composition.

Previous Research on the Tempe Volcanic Province

Volcanism in TVP. Tempe Terra can be divided into two surfaces consisting of older (Noachian) heavily cratered and fractured highland material to the east embayed by younger (Hesperian and Amazonian) volcanic material from the west (Wise, 1979; Moore, 2001). These plateaus and other highland material around Tharsis have been suggested to be older volcanic plains (Greeley and Spudis, 1981; Dohm et al., 2009). The presence of layers in the plateaus and several locations of lava flow fronts on the plateau support this hypothesis (Plescia, 1981). To the west the surface is smoother, less cratered and less fractured lowlands and is interpreted to be younger, volcanic material. Kipukas (islands of land surrounded by younger lava) of the fractured highland material can be seen in the younger, embaying volcanic material at the edge of the plateau. A variety of volcanic features have been reported in the province: 1) low shields, 2) cones, 3) domes, 4) fissures, 5) volcanic depressions, 6) rilles and 7) lava flows (Hodges, 1979, 1980; Plescia, 1981; Hodges & Moore, 1994; Sakimoto, 2008; Hauber et al., 2009, 2011). These features are seen on both surfaces but are not evenly distributed. To the west, they are more numerous and are often found in clusters, while to the east, they are less common and more likely to be isolated. Recently published CSFD modeled ages for low shields in Tharsis give ages between 190 Ma and 970 Ma for nine TVP low shields: compared to other clusters of low shields, TVP shields are older than those around the Tharsis Montes and younger than those in Syria Planum (Hauber et al., 2011).

Tectonism in TVP. Radial and concentric faults in the Tharsis province were first identified in Mariner photographs (Carr et al., 1973) and observed to belong to two populations, faults fanning to the northeast into Tempe Terra, and another less developed population fanning to the southwest. These fractures were thought to be the result of updoming of the crust and the fractures were thought to control the location of the volcanoes (Carr, 1974). More recent work by Anderson et al. (2001) classified the faults around Tharsis based on age and causative stress field into five main stages, two of which have fractured Tempe Terra. The oldest, and most active stage occurred in the Noachian and in a younger stage in the Early Hesperian. Tectonic features were categorized based on morphology (simple, complex, presence of pit chains, degradation state) and dimensions. Scott and Dohm (1990) studied faulting in Tempe Terra and identified eight distinct episodes of faulting in the region. Relative ages were determined based on crosscutting relationships and morphologic appearance. Stress fields are centered around central Tharsis Rise, Alba Patera, and various areas of magma intrusions producing graben with orientations of SW-NE, NW-SE, and N-S. They date the faulting as occurring from the Noachian through the Amazonian. Recent work by Neesemann et al. (2010) has CSFD model age dated tectonic activity in Tempe Terra to as young as 800 Ma by dating superposed lava flows. Other have suggested the radial graben are surface manifestations of near surface magma intrusions (dikes) and based on modeling, magma pressure, rather than regional stress is responsible for some if not all of the graben (McKenzie, 1999; Wilson and Head, 2002). While graben with SW-NE, N-S, and NW-SE orientations are seen on the older plateau material, it is only the SW-NE population that is visible on the younger embaying volcanic material.

Research Approach

The first component of this research includes production of a volcanic and structural map of the southwestern extent of Tempe Terra, from 95° to 84° W longitude to 30° to 45° N latitude. This was done using a mosaic of THEMIS Day IR images at a scale of 1:1,000,000. Units from Moore (2001) were used and only new volcanic vents are added.

The second component of this research included collecting morphometric data for the identified vents using gridded MOLA data at a resolution of 128 pix/deg and CTX images where available and THEMIS VIS images if not in a geographic information system (GIS) environment.

The third component of this research included counting craters and using CSFD to determine modeled ages for the identified vents. Once these data were collected, morphologic, spatial, and temporal trends could be identified.

This work improves upon previous mapping of Tempe Terra by increasing the number of identified vents, making morphometric measurements, and determining CSFD model ages for most vents. This was possible through the use of a 100 m/pix basemap (THEMIS Day IR) supplemented with MOLA elevation (1 km/pix), THEMIS VIS (18 m/pix), and CTX (6 m/pix) data.

Chapter 2

VOLCANIC MAP OF WESTERN TEMPE TERRA

Methodology

To identify and map the units and structures in the TVP, a base map was made by mosaicking THEMIS Day IR images and resizing to a scale of 1:1,000,000 (spatial resolution: 100 m/pixel). Images covering the TVP were identified using a planetary GIS tool called Java Mission-planning and Analysis for Remote Sensing (JMARS) (Christensen et al., 2009). Raw images were processed using ISIS (Torson and Becker, 1997) and mosaicked using an open source software package called DaVinci, which is maintained by the Mars Space Flight Facility at Arizona State University (http://davinci.asu.edu). The base map (Figure 4) was printed on a large format printer and tracing paper was placed over the map. Using methods described in Wilhelms (1990), outcrops, structures (e.g., graben and ridges), craters, and volcanic vents were mapped.

JMARS was used to identify higher resolution CTX images of each volcanic vent and ISIS was used to process the CTX images. The CTX images were then imported into ArcMap 10.0 and spatially co-registered to the MOLA 128 pixel/degree gridded data product (Smith et al., 2003). Using MOLA data, a profile for the vent was generated, orientated in the direction of the summit crater(s). If the summit pit crater(s) were not linear, then the profile was drawn in the SW-NE direction because of the previously suggested structural control of the graben on volcanic activity. A second profile was generated orthogonal to the first profile intersecting it at the vents summit. From these two profiles, four measurements were made for the volcano diameter, crater diameter, flank slope, and relief. These values were then used to calculate other characteristics for each volcano (Table 1), including aspect ratio (height to basal diameter), shield circularity, crater circularity, volume (using a simple cone model), area (based on average diameter), and crater diameter to basal diameter ratio.

Crater counts were performed on CTX images where available and when not available on THEMIS VIS images using ArcMap 10. Crater diameters and counting areas were measured using CraterTools software (Kneissl et al., 2011) and age determinations were made using CraterStats software (Michael & Neukum, 2010), applying Mars production and chronologies functions of Ivanov (2001) and Hartmann & Neukum (2001). Using crater counts to determine the age of a surface has been described in many papers (e.g., Hartmann et al., 1981; Hartmann & Neukum, 2001; Neukum & Hiller, 1981; Ivanov, 2001); the method attempts to fit the observed crater size-frequency distribution for a surface with a known crater production function obtained from a reference surface, and to use that fit to find a crater density for a standard crater diameter, and to convert that density to a model age (Ga) using a chronology function that has been calibrated with radiometrically dated lunar samples. Because this method is based on lunar samples and not martian samples, the different surface properties, planetary variables, and bolide populations must be accounted for by adjusting the chronology functions (Hartmann, 2005; Ivanov, 2001). Resurfacing by lava flows and gradational processes can change the crater population on a surface by covering or eroding smaller diameter craters. This process is observable on a cumulative crater frequency plot as a change in slope (kink) between two isochrons, for which a correction can be made (Michael & Neukum, 2010).

The accuracy of this method is a debated topic (Hartmann, 1971; Hartmann and Neukum, 2001; McEwan et al., 2005) but relative ages can still provide useful information.

Results

Units. Because this work focuses on the younger volcanic units, and not the older units they may embay, existing unit descriptions from Moore (2001) are used for the older plateau material.

Volcanoes.

Low Shields (LS). These features have some or all of the following characteristics: low relief (< 2 degree slopes, often < 0.5 degrees), summit crater(s), radial texture or smooth flanks, discontinuous channels, leveed channels, visible lobate flow(s) originating at the summit, and proximal to lobate flows on some (Figure 5). These features are interpreted to be low shields as defined by Greeley (1982). These features may be conical or have low, broad ridges that have an elliptical base. Average flank slopes are commonly less than one degree and flank steepening near the summit is present.

Linear Low Shields (LLS). These features have the same characteristics as low shields but are distinguished by the ratio between the semimajor axis of the crater and the semiminor axis of the volcano (ratio > 5; Figure 6). This classification is somewhat subjective and only three volcanoes were classified as

Table 1

Morphometric Properties of Identified Vents in the TVP. Sma = semimajor, Smi = semiminor, Y = yes, N = no, I = indeterminate, d = crater semiminor diameter, D = basal semiminor diameter, Volume is calculated as $V=1/3*pi*r^2h$, and Age = CSFD modeled age.

Vent	Type	Basal Sma diam. (m)	Basal Smi diam. (m)	Elevation (m)	Relief (m)	Slope (deg.)	Aspect Ratio	Embayed	Topo. Controlled	Crater Sma diam. (m)	Crater Smi diam. (m)	Crater Circularity	d/D	Volume (km^3)	Age (Ga)
TempeTe_01_ASU_CTX_TP	LS	24523	17835	649	80	0.44	0.004	Y	I	590	490	0.83	0.03	9.4	2.3
TempeTe_01_PJ_CTX	LS	70152	54148	961	248	0.49	0.004	Y	I	1780	1050	0.59	0.02	250.8	0.76
TempeTe_02_ASU_CTX_TP	LS	45336	75492	1279	305	0.40	0.005	Y	Y	2780	920	0.33	0.01	291.5	1.8
TempeTe_02_PJ_CTX	LS	14732	19776	701	62	0.44	0.004	Y	I	613	553	0.90	0.03	4.8	0.68
TempeTe_03_ASU_CTX_TP	LS	36543	20088	916	150	0.70	0.005	Y	Y	1760	320	0.18	0.02	31.5	0.67
TempeTe_03_PJ_CTX	LS	52510	31249	800	174	0.54	0.004	Y	Y	4163	3464	0.83	0.11	80.1	0.69
TempeTe_04_ASU_CTX_TP	LS	31933	33552	1086	120	0.43	0.004	Y	Y	709	454	0.64	0.01	33.7	1
TempeTe_04_PJ_CTX	LS	15607	19751	557	43	0.29	0.002	Y	Y	969	441	0.46	0.02	3.5	0.3
TempeTe_05_ASU_CTX_TP	LS	32856	39997	906	151	0.53	0.004	Y	Y	690	600	0.87	0.02	52.3	1.7
TempeTe_05_PJ_CTX	LS	27257	22015	1364	243	1.26	0.010	N	Y	1673	973	0.58	0.04	38.7	0.19
TempeTe_06_ASU_CTX_TP	F	200860	34905	1203	47	0.23	0.000	N	Y	NA	NA	NA	NA	170.1	0.97
TempeTe_06_PJ_CTX	S	5601	6930	1336	162	2.98	0.026	N	Y	639	540	0.85	0.08	1.7	0.68
TempeTe_07_PJ_CTX	LS	17474	13646	1461	155	1.29	0.010	N	Y	1005	525	0.52	0.04	9.8	0.58
TempeTe_07_ASU_CTX_TP	LS	77179	32234	1047	245	0.52	0.004	Y	Y	NA	NA	NA	NA	192.2	0.36
TempeTe_08_ASU_CTX_TP	LS	15575	14773	786	40	0.31	0.003	Y	Y	590	512	0.87	0.03	2.4	0.68
TempeTe_08_PJ_CTX	LS	51166	45055	1297	337	0.83	0.007	Y	N	661	521	0.79	0.01	204.3	0.43
TempeTe_09_ASU_CTX_LM_TP	LS	4469	10082	1359	83	1.46	0.011	Y	Y	939	550	0.59	0.05	1.1	0.4
TempeTe_09_PJ_CTX	LS	73536	40921	1112	206	0.49	0.004	Y	N	4092	980	0.24	0.02	176.8	0.97
TempeTe_10_ASU_CTX_LM_TP	LS	6829	11339	1348	88	1.04	0.010	Y	Y	434	136	0.31	0.01	1.9	0.4
TempeTe_11_ASU_CTX_LM_TP	LS	5541	4994	1231	31	0.69	0.006	N	N	360	320	0.89	0.06	0.2	0.35
TempeTe_12_ASU_CTX_LM	LS	3562	4021	1227	21	0.70	0.005	I	Y	167	142	0.85	0.04	0.1	NA
TempeTe_13_ASU_CTX_LM_TP	LS	51798	29848	1323	182	0.53	0.004	I	Y	2413	595	0.25	0.02	79.6	0.43
TempeTe_14_ASU_CTX_LM_TP	LS	19816	18939	1316	99	0.59	0.005	N	Y	1050	420	0.40	0.02	9.7	1.8
TempeTe_15_ASU_CTX_LM_TP	LLS	20440	34293	1097	116	0.37	0.004	N	N	8660	1039	0.12	0.03	22.8	0.63
TempeTe_16_ASU_CTX_LM_TP	LS	86003	62338	980	128	0.20	0.002	N	Y	1453	676	0.47	0.01	184.1	0.89
TempeTe_17_ASU_THEMIS_LM	LLS	21957	9629	933	27	0.30	0.002	Y	N	14086	398	0.03	0.04	1.7	0.59
TempeTe_18_ASU_CTX_LM	LS	26582	15063	931	39	0.24	0.002	I	N	1555	600	0.39	0.04	4.4	0.34
TempeTe_19_ASU_CTX_LM	LS	38581	19056	956	123	0.47	0.004	I	Y	NA	NA	NA	NA	26.8	0.71
TempeTe_20_ASU_CTX_LM	LS	4999	4855	765	37	0.84	0.008	I	Y	178	157	0.88	0.03	0.2	NA
TempeTe_21_ASU_CTX_LM	LS	32927	22797	950	106	0.45	0.004	N	Y	390	380	0.97	0.02	21.5	0.45
TempeTe_22_ASU_CTX_LM	LS	36794	25302	884	193	0.73	0.006	I	Y	811	450	0.55	0.02	48.7	0.16
TempeTe_23_ASU_CTX_LM	LS	42257	41972	1075	179	0.53	0.004	Y	Y	750	710	0.95	0.02	82.8	0.53
TempeTe_24_ASU_CTX_LM	LS	20193	22640	1086	120	0.95	0.006	Y	Y	5420	1095	0.20	0.05	14.4	0.3
TempeTe_26_ASU_CTX_LM	LS	11557	5871	797	31	0.41	0.004	Y	Y	1580	978	0.62	0.17	0.6	0.73
TempeTe_25_ASU_CTX_LM	LS	18878	13319	884	60	0.48	0.004	I	Y	2075	230	0.11	0.02	4.1	0.5
TempeTe_27_ASU_CTX_LM	LS	42457	42391	817	99	0.36	0.002	Y	Y	13023	600	0.05	0.01	46.5	0.89
TempeTe_28_ASU_CTX_LM	LS	47350	15717	1211	130	0.53	0.004	Y	Y	1240	470	0.38	0.03	33.8	1.1

TempeTe_30_ASU_CTX_LM	LS	20955	20502	990	76	0.42	0.004	Y	N	1264	536	0.42	0.03	8.5	2
TempeTe_31_ASU_CTX_LM	F	6385	11457	976	19	0.33	0.002	N	Y	NA	NA	NA	NA	0.4	NA
TempeTe_32_ASU_CTX_LM	LS	21088	16530	1023	77	0.45	0.004	Y	NA				0.00	7.1	0.98
TempeTe_33_ASU_CTX_LM	LS	14735	12533	809	54	0.43	0.004	N	Y	243	225	0.93	0.02	2.6	0.12
TempeTe_34_ASU_CTX_LM	LS	9597	8898	1239	65	0.79	0.007	I	Y	628	294	0.47	0.03	1.5	2.4
TempeTe_35_ASU_CTX_LM	LS	24500	19558	1096	138	0.76	0.006	N	Y	1233	315	0.26	0.02	17.5	0.19
TempeTe_36_ASU_CTX_LM	LS	10929	32547	1012	74	0.38	0.003	Y	Y	1365	1129	0.83	0.03	9.2	0.22
TempeTe_37_ASU_CTX_LM	LS	20258	12378	1096	99	0.74	0.006	N	Y	874	553	0.63	0.04	6.9	0.34
TempeTe_38_ASU_CTX_LM	F	NA	NA	897	NA	NA	NA	N	N	NA	NA	NA	NA	NA	0.19
TempeTe_39_ASU_CTX_LM	LS	10966	6797	759	83	1.13	0.009	N	Y	1148	286	0.25	0.04	1.7	0.59
TempeTe_40_ASU_CTX_LM	S	5440	5482	843	118	2.46	0.022	Y	I	448	352	0.79	0.06	0.9	0.3
TempeTe_41_ASU_CTX_LM	S	15400	7631	760	172	2.01	0.015	N	Y	1980	488	0.25	0.06	6.0	1.5
TempeTe_42_ASU_CTX_LM	LS	65991	32288	1015	274	0.72	0.006	Y	Y	1318	852	0.65	0.03	173.3	0.66
TempeTe_43_ASU_CTX_LM	LLS	32326	20324	828	88	0.43	0.003	N	Y	1640	324	0.20	0.02	15.9	0.31
TempeTe_44_ASU_THEMIS_LM	?	15891	14209	318	34	0.31	0.002	N	N	976	777	0.80	0.05	2.0	0.59
TempeTe_45_ASU_CTX_LM	LS	14334	13760	648	112	0.94	0.008	Y	I	710	391	0.55	0.03	5.8	0.96
TempeTe_46_ASU_CTX_LM	S	4950	6198	350	104	2.98	0.019	Y	Y	1616	563	0.35	0.09	0.8	0.73
TempeTe_47_ASU_CTX_LM	LS	3721	6241	250	40	0.82	0.008	Y	I	1101	577	0.52	0.09	0.3	NA
TempeTe_48_ASU_CTX_LM	LS	16535	17388	729	64	0.49	0.004	I	N	1246	460	0.37	0.03	4.8	NA
TempeTe_50_ASU_CTX_LM	LS	25423	35622	347	60	0.21	0.002	I	N	972	800	0.82	0.02	14.5	1.4
TempeTe_51_ASU_CTX_LM	LS	23043	29570	331	56	0.28	0.002	I	N	597	424	0.71	0.01	10.2	0.38
TempeTe_52_ASU_CTX_LM	C	783	646	870	NA	NA	NA	I	N	480	451	0.94	0.70	NA	NA
TempeTe_53_ASU_CTX_LM	C	621	552	695	NA	NA	NA	I	I	327	231	0.71	0.42	NA	NA
TempeTe_54_ASU_CTX_LM	LS	16999	34052	1038	182	0.98	0.007	Y	Y	559	460	0.82	0.01	31.1	0.72
TempeTe_55_ASU_CTX_LM	LS	11785	15380	834	65	0.64	0.005	Y	Y	351	159	0.45	0.01	3.1	0.55
TempeTe_56_ASU_CTX_LM	LS	12841	8286	825	47	0.59	0.004	I	Y	613	325	0.53	0.04	1.4	0.48
TempeTe_57_ASU_CTX_LM	LS	10048	9391	882	67	0.87	0.007	Y	Y	874	518	0.59	0.06	1.7	0.63
TempeTe_58_ASU_CTX_LM	LS	13599	9019	1386	145	1.69	0.013	Y	Y	876	543	0.62	0.06	4.9	0.32
TempeTe_60_ASU_CTX_LM	LS	11880	8188	849	29	0.39	0.003	N	Y	1440	495	0.34	0.06	0.8	0.21
TempeTe_61_ASU_THEMIS_LM	C	780	730	1065	NA	NA	NA	I	N	191	172	0.90	0.24	NA	NA
TempeTe_62_ASU_THEMIS_LM	C			1052	NA	NA	NA	I	N	NA	NA	NA	NA	NA	NA
TempeTe_63_ASU_THEMIS_LM	C	228	215	1080	NA	NA	NA	I	N	93	83	0.89	0.39	NA	NA
TempeTe_64_ASU_THEMIS_LM	C	656	569	1086	NA	NA	NA	I	N	311	199	0.64	0.35	NA	NA
TempeTe_65_ASU_CTX_LM	LS	34575	13246	881	70	0.31	0.003	N	Y	421	247	0.59	0.02	10.5	0.46
TempeTe_66_ASU_CTX_LM	C	304	268	681	NA	NA	NA	Y	N	200	147	0.74	0.55	NA	NA
TempeTe_67_ASU_CTX_LM	C	113	97	699	NA	NA	NA	I	N	40	38	0.95	0.39	NA	NA

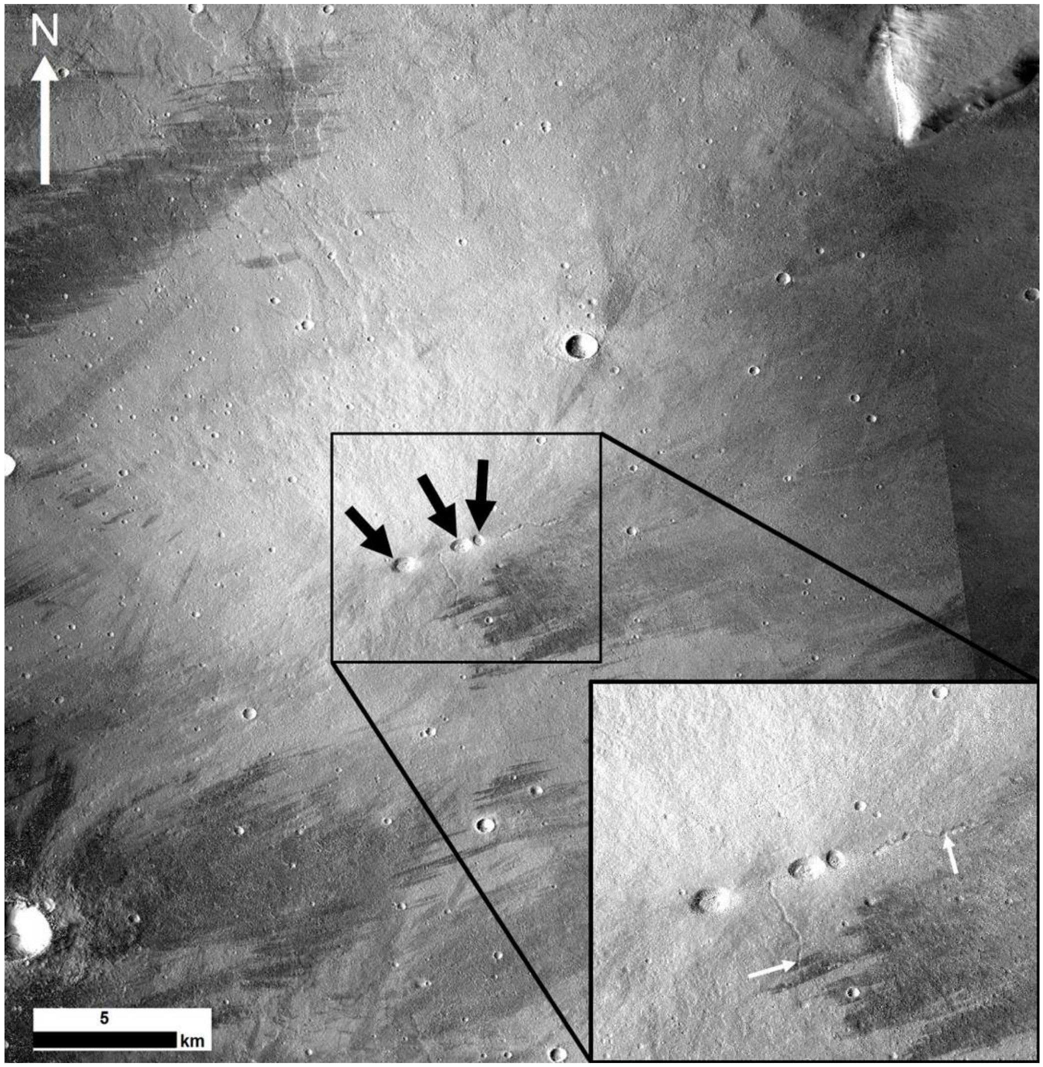

Figure 5. Low shield with multiple summit craters (black arrows). Very low relief makes distinguishing the southern contact impossible in this image. Multiple lobate flows are seen to the north. Insert shows channels near the summit (white arrows) (CTX image P20_008867_2168_XI_36N088W).

such. These are interpreted to form along a fissure but unlike low shields, eruptions have not coalesced to a central source.

Shields (S). These features have the same characteristics as the low shields except that they have average flank slopes greater than 2 degrees. Two of the four identified shields with this characteristic are embayed by younger

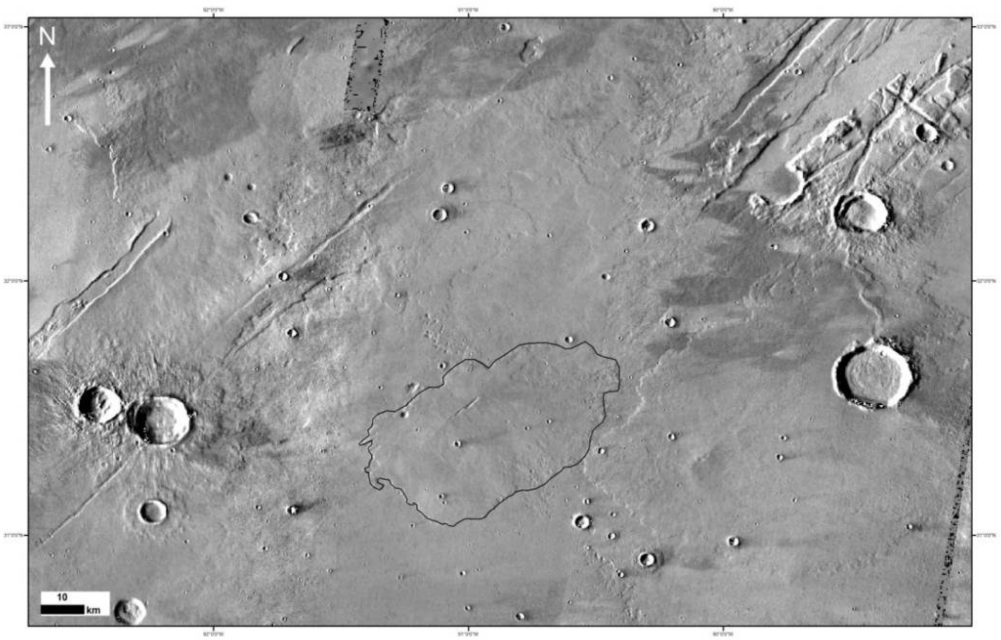

Figure 6. Black outline around a shield classified as a Linear Low Shield (LLS). Note elongate linear summit depression. To the east is a low shield (LS) and above is a fissure (F) fed eruption. Also visible are graben trending SW-NE as well as an older set trending NW-SE. Background is a mosaic of THEMIS day IR images.

lava, such that the steeper slopes may represent steepening near the summit and not the average flank slope for the original edifice (Figure 7). These features are interpreted to be similar to Icelandic shields as defined by Pike (1978).

Cones (C). These features have smaller diameters than the shield volcanoes, visibly steeper flank slopes (they are too small to measure using MOLA data), and much higher crater diameter to basal diameter ratios (Figure 8). Only eight examples of this type of feature were found, although that is likely due to a resolution bias. These are interpreted to be similar to cinder cones.

Other. These features have a variety of morphologies and are not easily classified. Some have morphologies intermediate between impact craters and

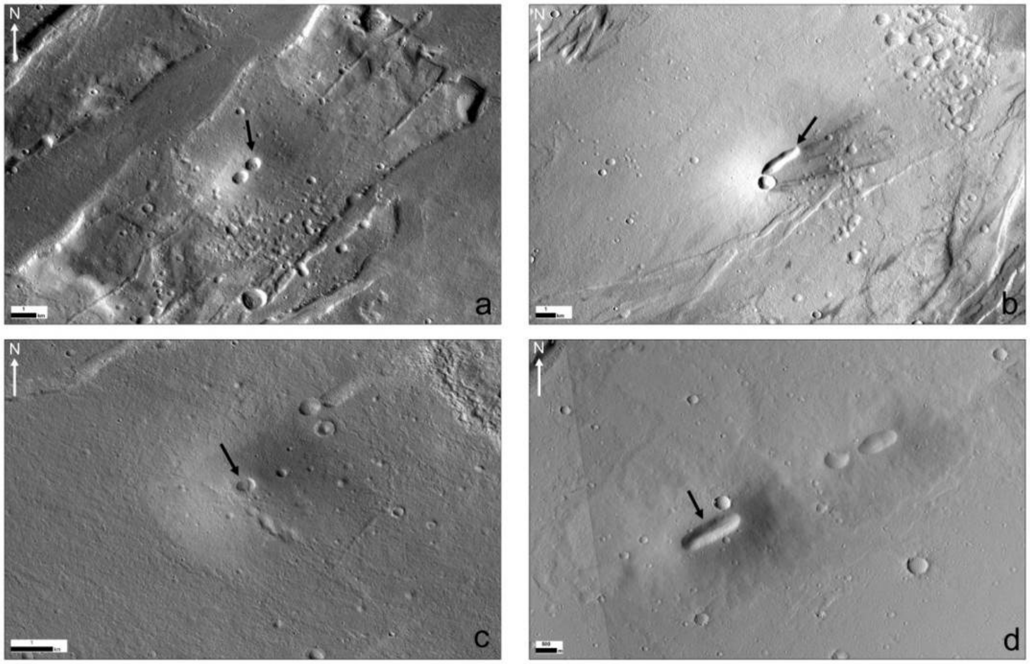

Figure 7. Examples of the volcanoes with average flank slopes greater than 2 degrees and classified as Shields (S). Relief is easier to see on these than those classified as LS (Figure 4). (a) One of the few shields found on the older fractured plateau material (CTX image P03_002182_2159_XN_35N088W). (b) Elongate summit crater with orientation similar to the graben (CTX image P01_001364_2162_XI_36N085W). (c) Cone shaped shield that has been embayed. Note the strange morphology of the craters to the NE and E (CTX image P05_002894_2165_XI_36N086W). (d) Another embayed shield similar to (b) and has a proximal low shields to the NE. Both shields have elongate central craters trending in the orientation of the graben (CTX image B02_010225_2134_XN_33N084W).

volcanic craters (Figure 9). Some are linear depressions with sloping embankments (Figure 10). These features are interpreted to be potentially volcanic based on proximity to other volcanic features, with characteristics similar to maars and spatter ramparts. Rilles (Figure 11) and fissure fed flows (Figure 8) are also seen in the area.

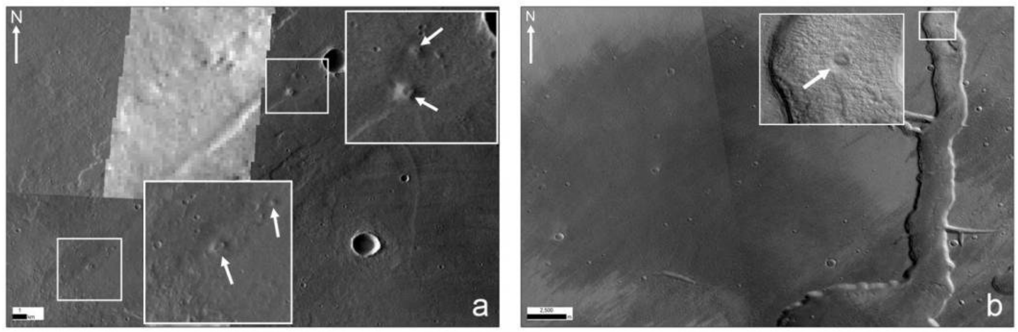

Figure 8. Examples of possible cinder cones. (a) Four possible cinder cones located on a Fissure (F) fed eruption. Cones are located over a linear central depression interpreted to be a graben (THEMIS images V09565007 and V30605007). (b) Possible cinder cone in a sinuous rille (CTX image P15_006784_2196_XN_39N090W).

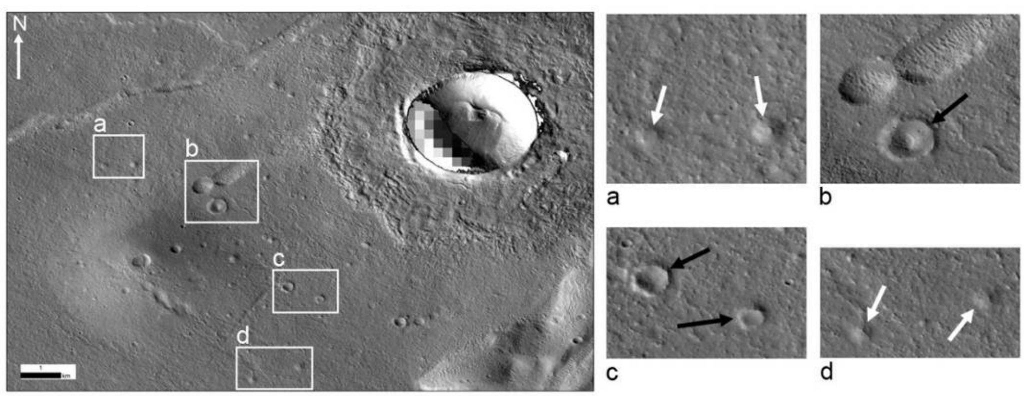

Figure 9. Other possible volcanic features. Based on proximity to the shield volcano in the lower left corner interpreted to be maars (b and c) and domes or eroded cinder cones (a and d). (CTX image P05_002894_2165_XI_36N086W)

Trends.

Temporal trends. The spatial distribution of ages is shown in Figure 12. Ages appear loosely to trend younger to the northeast for shields younger than 800 Ma, whereas those older than 800 Ma are found through-out the TVP except for the NE area. Some low shields appear to be aligned along graben and are

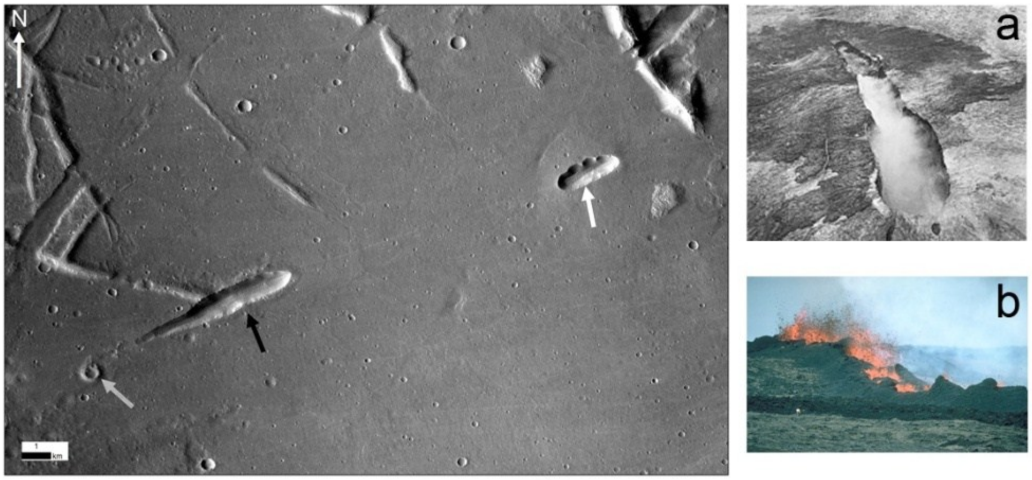

Figure 10. More examples of other types of vents (CTX image G02_018928_2133_XN_33N087W). The white arrow points to a depression that is similar to (a), the summit vent of Mauna Ula, Hawaii, in May 1973 (photograph by R.T. Holcomb; from Carr and Greeley, 1980). The black arrow identifies a feature that characteristics similar to a spatter rampart (b) on Mauna Loa, Hawaii, in March 1984 (photograph by J.D. Griggs). The grey arrow points to a feature that could be a cinder cone or an eroded impact crater.

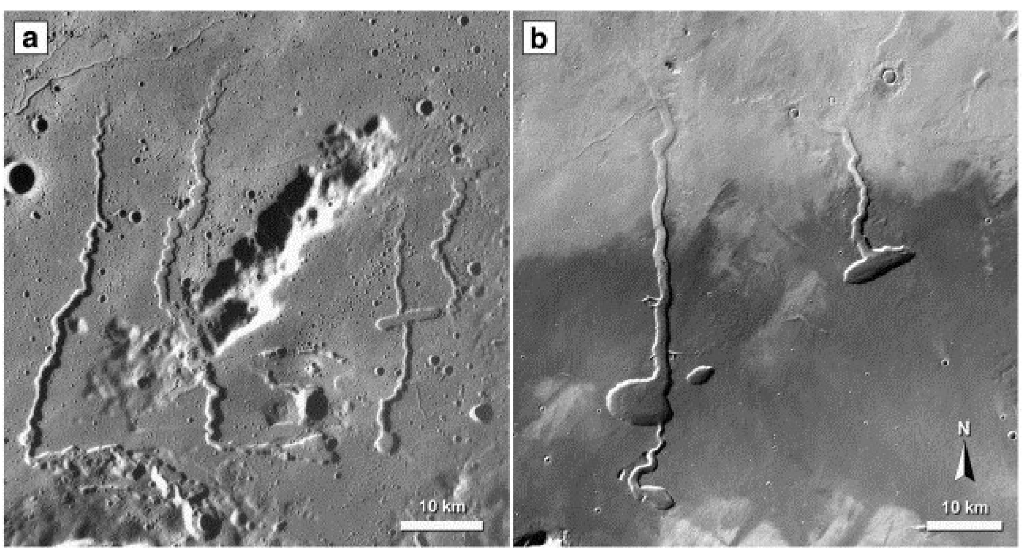

Figure 11. Topographic depressions with sinuous rilles. (a) Sinuous rilles seen on the Moon (Apollo 15 image M-2082). (b) Nearly identical features seen in the TVP (HRSC image H1594_0000). Images from Hauber et al., 2009.

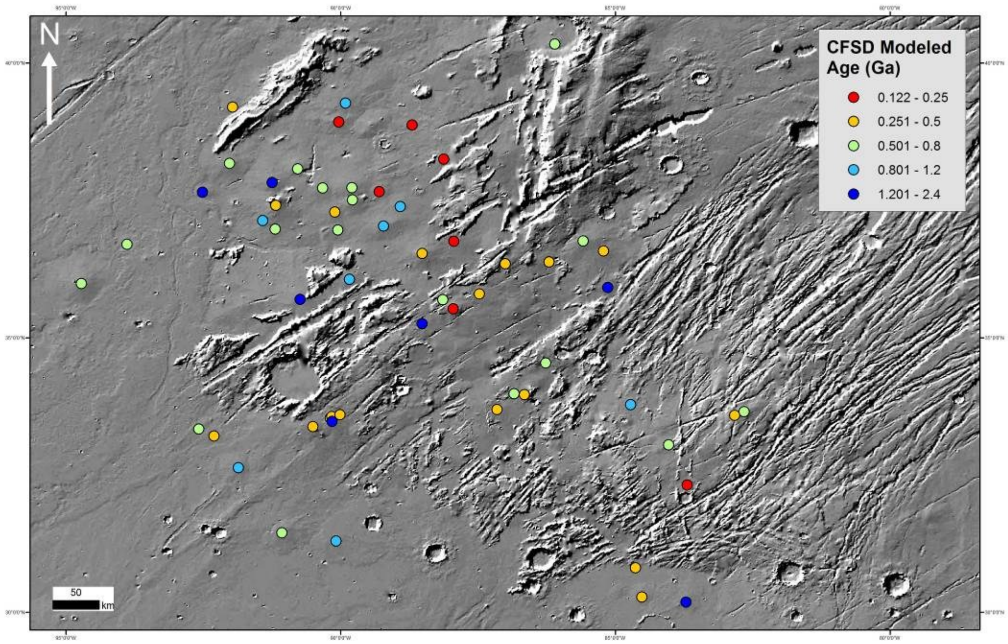

Figure 12. Ages of the shields in the TVP on a MOLA shaded relief background.

roughly contemporaneous in age (Figure 12). There appears to be a very weak correlation between the average flank slope and age such that slope decreases with increasing age (Figure 13).

Spatial trends. Those shields with the lowest slopes, less than 0.3 degrees, are found on the western edge of Tempe Terra, whereas those with the steepest slope are more common further east in Tempe Terra (Figure 14). All but one of the volcanoes classified as a shield is located in the large NW trending fault block found in the middle of the mapping area (Figure 14). Groups of shields sometimes have a NE-SW orientation, parallel or sub-parallel to the graben (Figures 7, 12).

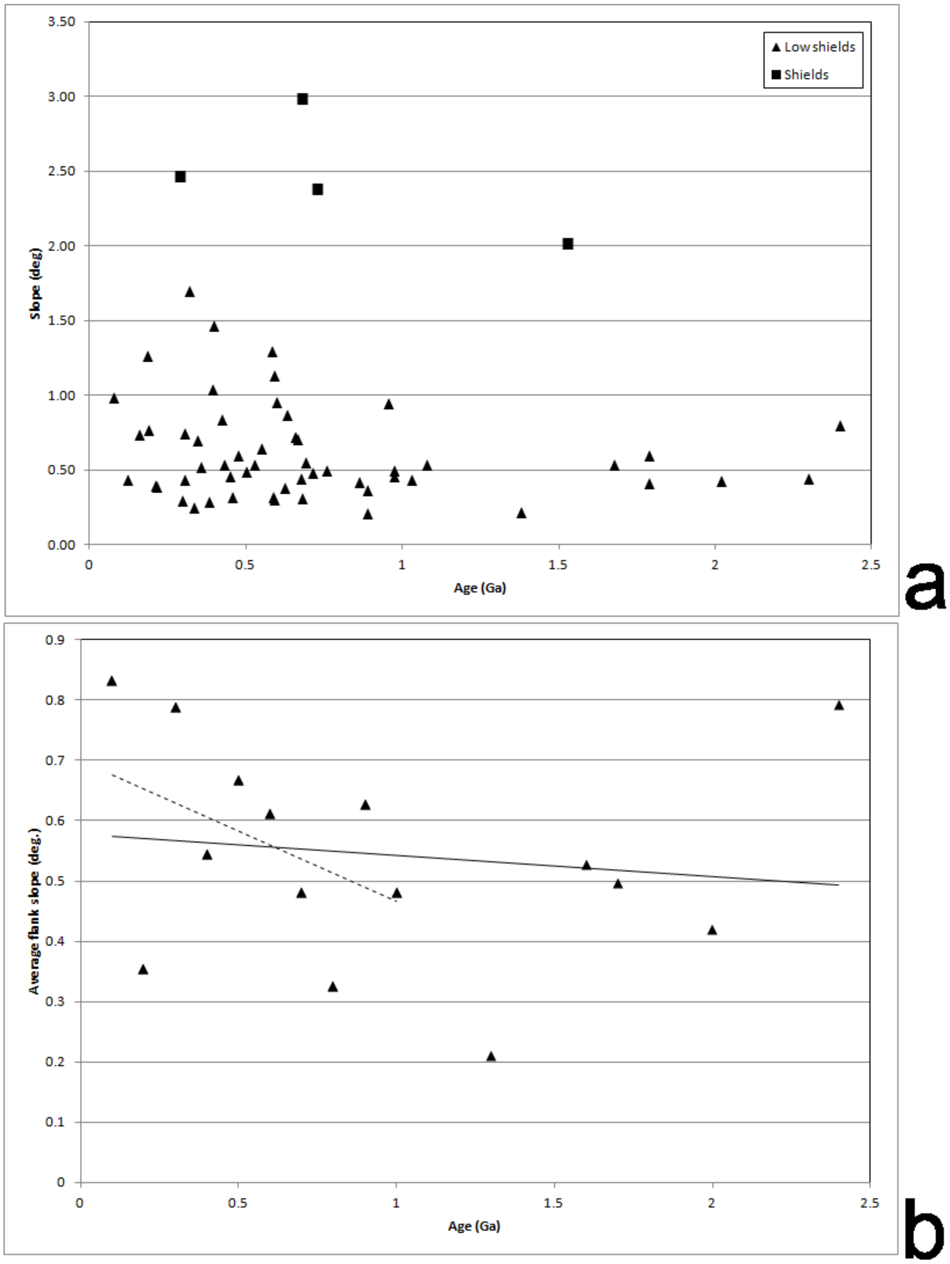

Figure 13. Shield slopes in the TVP. (a) Shields older than 1 Ga have slopes around 0.5 degrees. For shields younger than 1 Ga, many different slopes are represented. Linear low shields are included with low shields. (b) Average flank slope for all shields in 100 My bins. Solid trendline is for all ages and the dashed line is for shields 1 Ga and younger. Both show a decrease in slope with age. Error bars are not shown; however, for most shields they are smaller than 100 My. Older shields (> 1 Ga) and shields where ages were determined from a minimal number of craters (< 10) have the largest error bars (as much as 700 My).

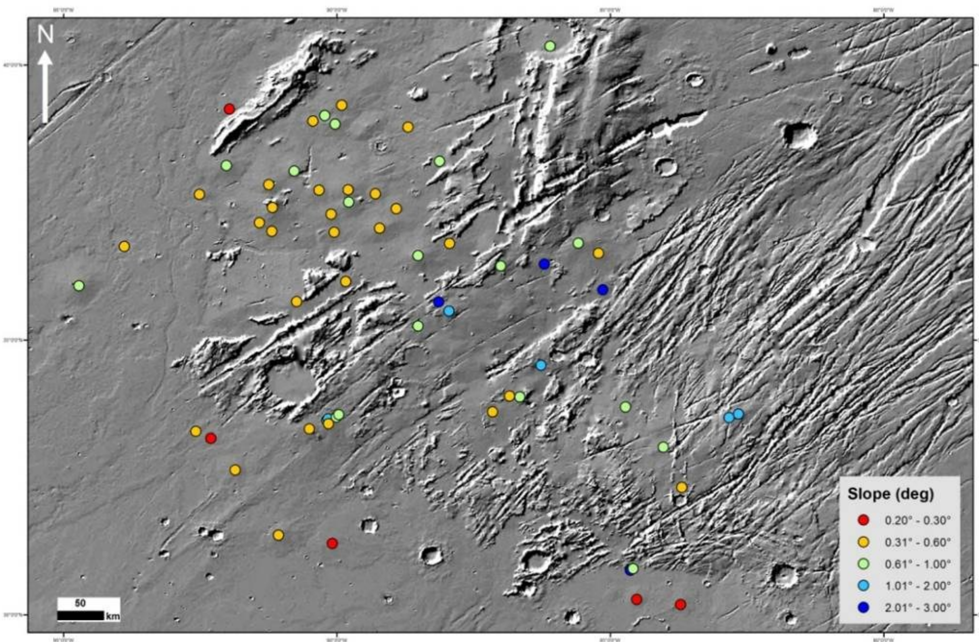

Figure 14. Spatial distribution of slopes for all shields in the TVP on a MOLA shaded relief background.

Morphologic trends. The most voluminous low shields are more common at higher elevations (Figure 15). Those volcanoes at higher elevations also have larger average flank slopes (Figure 16). Shield volcanoes have the largest average flank slopes but are among the smallest diameter volcanoes in the TVP (Figure 17). For low shields, although there is no correlation between the ratio of the diameter of the crater to the basal diameter with basal diameter, the low shields do cluster together and are distinguishable from other shield classifications as described by Pike (1978) (Figure 18). There is a strong correlation between volume and area for the TVP low shields (Figure 19). The longest axis of the summit crater(s) for all shield types are often oriented NE-SW, similar to the dominant graben trend. Some low shields appear to be aligned along graben (Figures 5, 6,7a, 7b, 7d, 20). Only three fissure fed flows were positively

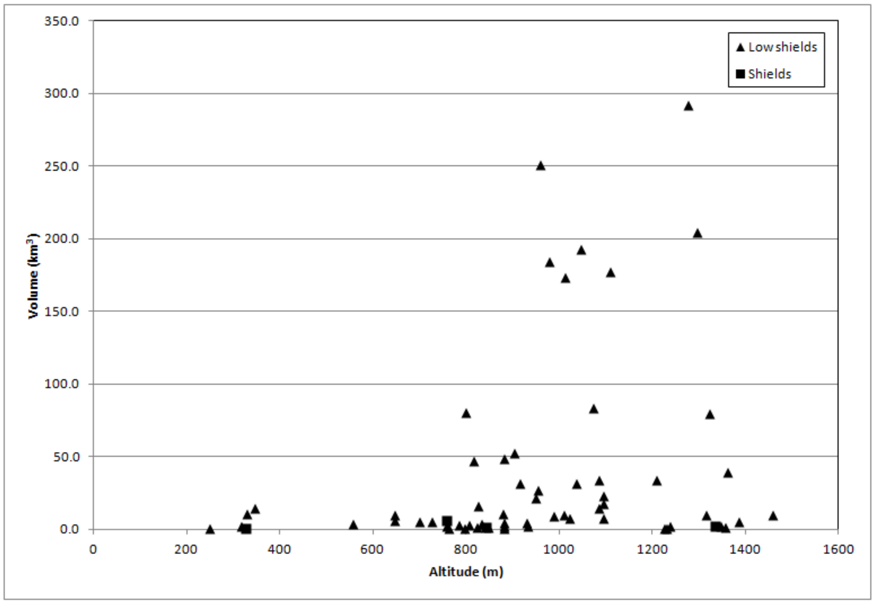

Figure 15. The most voluminous low shields are present at higher elevations.

identified but it is likely that more are present. Fissure fed flows were the most difficult to identify due to their very low relief and similar shape to graben.

Discussion and Implications

Temporal and spatial evolution. CSFD modeled ages for shields in the TVP indicate shield forming volcanism occurred throughout the area between ~1 and 2.4 Ga b.p. Subsequently, around 800 Ma, volcanic activity may have begun to migrate to the NE, with the youngest low-shields found in the northern- and eastern-most regions of the field. Based on the number of shields for a given age, activity quickly increased to a peak between 400 to 700 Ma and just as quickly, ceased activity between 400 to 120 Ma. It is likely that the younger shields have not only embayed, but also completely covered older edifices, obscuring their true numbers and characteristics. Some shields are superposed on graben, whereas graben crosscut other shields indicating tectonism has been long lived in the area.

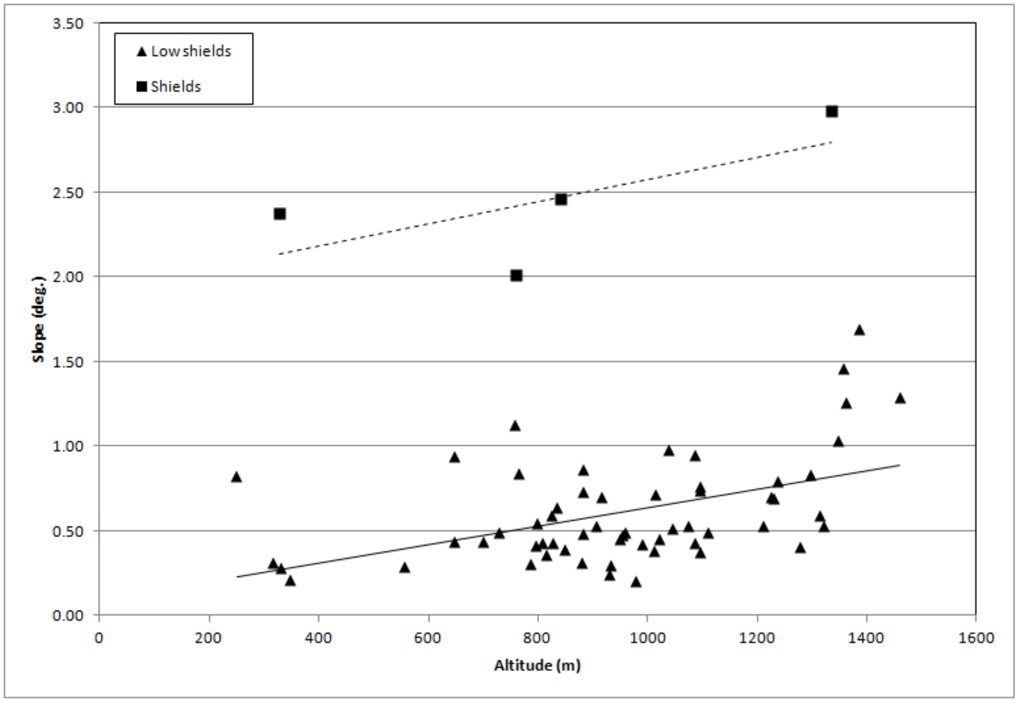

Figure 16. There is no strong correlation between average flank slope and elevation but there is a weak trend toward higher slopes at higher elevations. The solid trendline is for low shields while the dashed trendline is for shields.

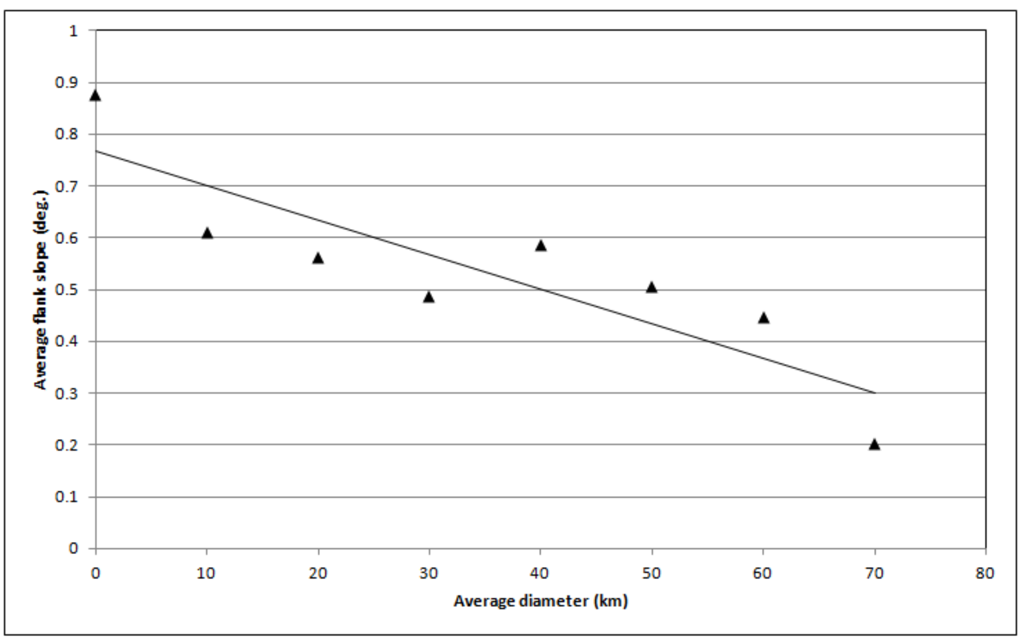

Figure 17. Average flank slope versus binned basal diameter.

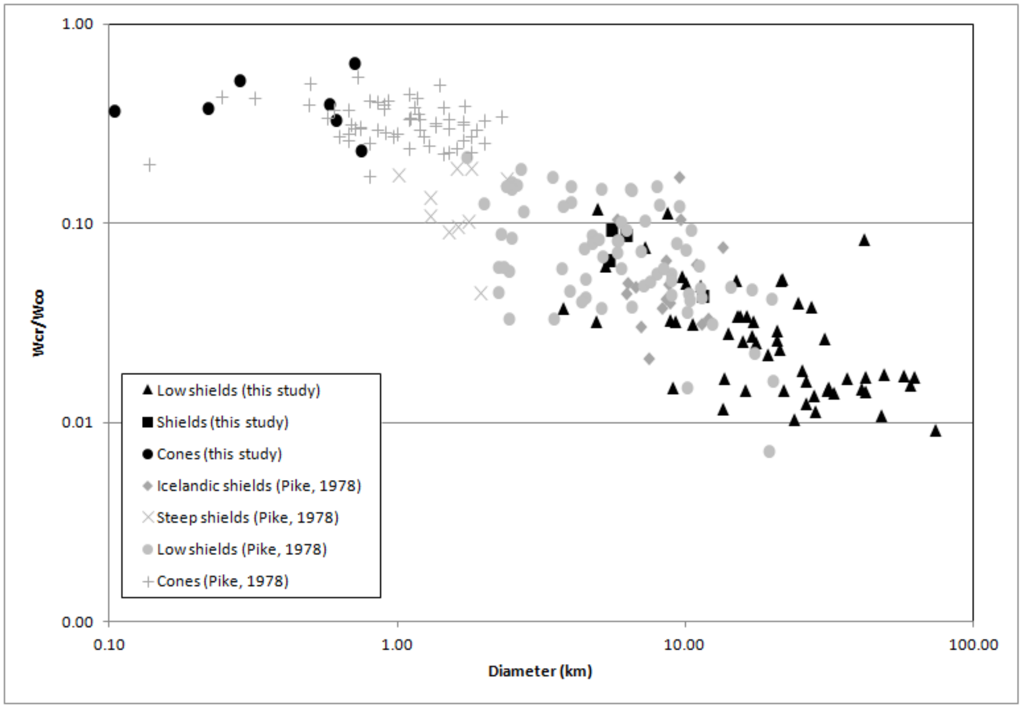

Figure 18. Ratio of crater diameter to basal diameter versus basal diameter. Includes data from this study as well as Pike (1978).

That the more voluminous low shields are often found at higher elevations may offer clues as to what is occurring below the surface. A greater overburden pressure on a magma chamber from a surface at a higher elevation may require a larger volume of magma be present in the magma chamber to generate the conditions (pressure or buoyancy) necessary to erupt. The most voluminous low shields also have low average flank slopes. Therefore, these low shields are indicative of eruptions with high rates of effusion rather than eruptions with lower rates of effusion that should result in edifices with steeper slopes. Volcanoes classified as shields with average flank slopes >2 degrees, tend to have small (<12 km) diameters, and are thought to have been formed by less voluminous eruptions and may owe their shape to the eruption of more viscous lava at lower rates of

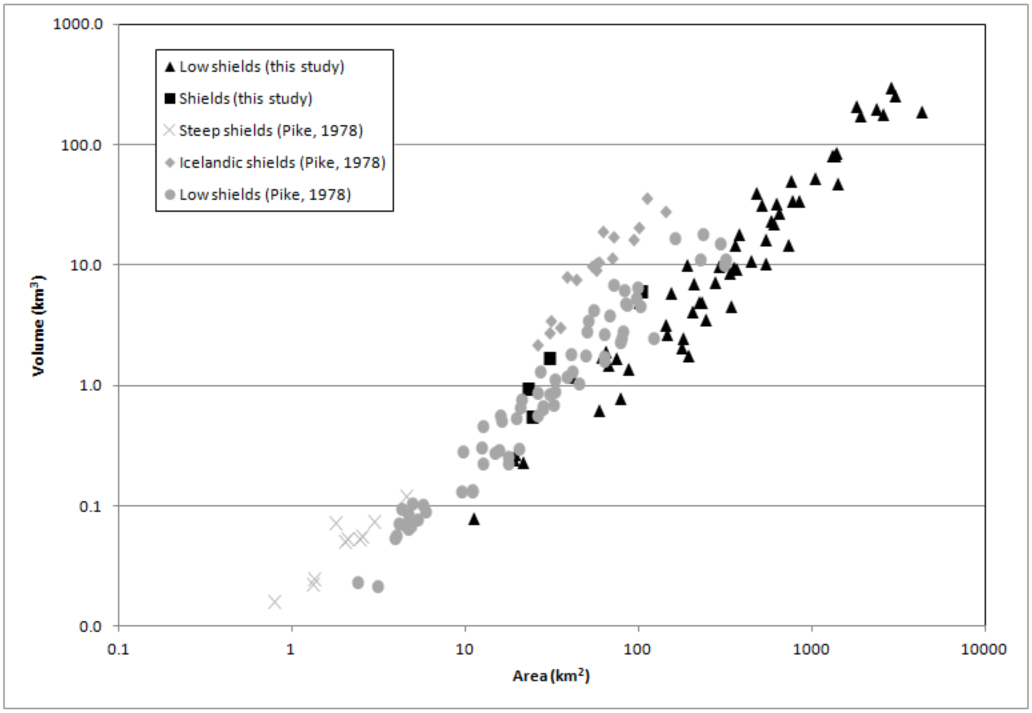

Figure 19. Volume versus area. The TVP shields are most similar to terrestrial shields classified by Pike (1978) as low shields although the plot slightly lower indicating lower flank slopes for a given area.

effusion. The younger shields also tend to have steeper average flank slopes which hints at some type of evolution of the system; either magma source pressure has decayed reducing effusion rates over time or the younger magmas have a different rheology (more viscous), possibly coming from a different source or simply representing a more crystallized, degassed version of the older magmas. Lower slopes on older shields are not thought to be due to erosion, either through fluvial or aeolian processes, due to the lack of erosional features. That the volume to area ratio (Figure 19) is very similar to low shields on Earth suggests a similar style of eruption. The fact that the TVP low shields plot at and slightly below their terrestrial counterparts suggests a higher effusion rate or lower viscosity due to planetary variables (Wilson and Head, 1994).

Comparison to previous work. These findings build upon previous work that compared the TVP to the Snake River Plains of Idaho (Plescia, 1981; Sakimoto et al., 2003) and to other fields of low shields (Hauber et al., 2009, 2011). TVP volcanoes have morphological characteristics similar to volcanoes on Earth and other low shields on Mars (Figures 18, 19, and 21). Derived ages for volcanic material in TVP indicate the shields formed contemporaneously with other low shields in Tharsis as well as the larger shields (Werner, 2009; Hauber et al., 2011). Mapped graben azimuths (Figure 22) agree with previous tectonic investigations in the TVP (Anderson et al., 2001; Scott and Dohm, 1990). The dominant NE-SW graben orientation reflects the most recent stress field in the area while older stress fields are represented by graben with W-E and NW-SE orientations. No lateral displacement is seen along the graben.

Implications for Tharsis. Many shields have linear vents (Figures 5, 6,7a, 7b, 7d, 20) that are aligned with the predominant orientation of the graben (Figure 22). This alignment is roughly radial to the center of Tharsis and suggests the graben and distribution of shields in the TVP are related to stresses caused by Tharsis volcanoes as suggested by Scott and Dohm (1990), McKenzie (1999) and Wilson and Head, (2002) . The migration of volcanic activity in the TVP towards the NE beginning approximately 800 Ma is roughly radial to Tharsis and could be the result of a changing stress field associated with Tharsis or a migration of the location of the dominant magma source. Large lava flows that Moore (2001) mapped as originating from the direction of Tharsis embay some of the older

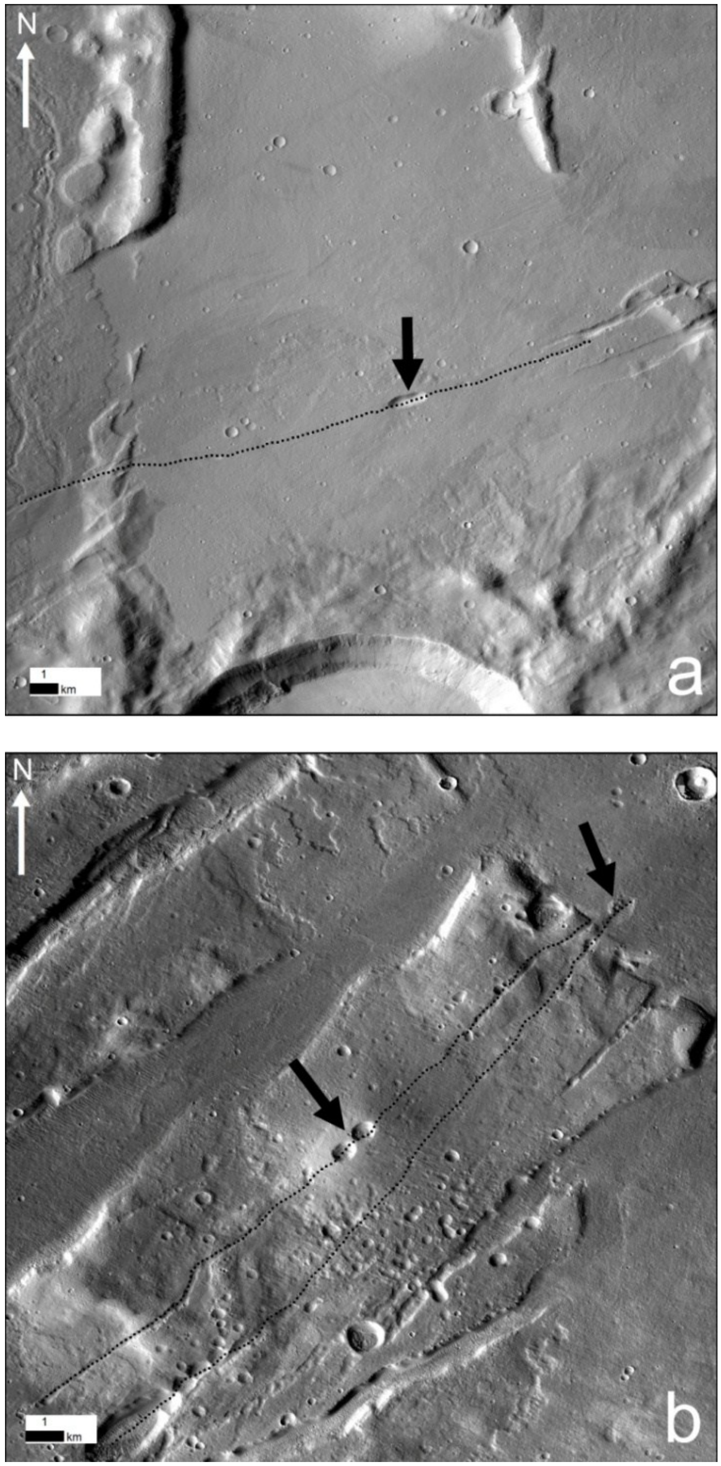

Figure 20. Shields (black arrows) superposed on graben (dashed lines). (a) Low shield superposed on a graben (CTX image P21_009236_2133_XN_33N083W). (b) Shield (left arrow) and low shield (right arrow) superposed over a graben. Lobate flows extend to the north (CTX image P03_002182_2159_XN_35N088W).

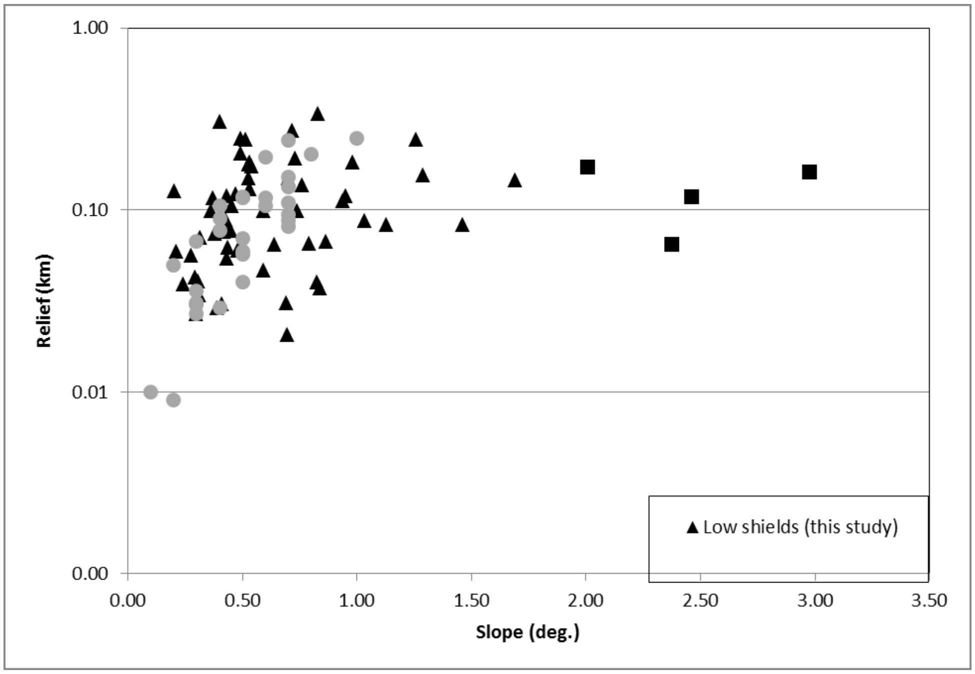

Figure 21. Relief versus average flank slope. Low shields and shields have no overlap and low shields in the TVP plot over those in Syria Planum (Baptista et al., 2008)

shields located in the SW portion of the TVP. This suggests that the SW extent of the TVP ceased activity before Tharsis, which may still be active.

Problematic elements and uncertainties. Although approximately sixty volcanic features were dated for this work, there are at least another twenty shields or low shields that were not dated and morphologically documented in the TVP. Ages and morphologies of these shields could support or refute the findings of this work. While absolute model ages for surfaces on Mars has been used for years to determine age relationships, the error bars associated with the derived ages is a hotly debated topic. Error bar size is largely a function of modeled age and the number of craters used to model the age. Most error bars are less than 100 My, although some of the older shields (e.g. one dated at 1.9 Ga) has an

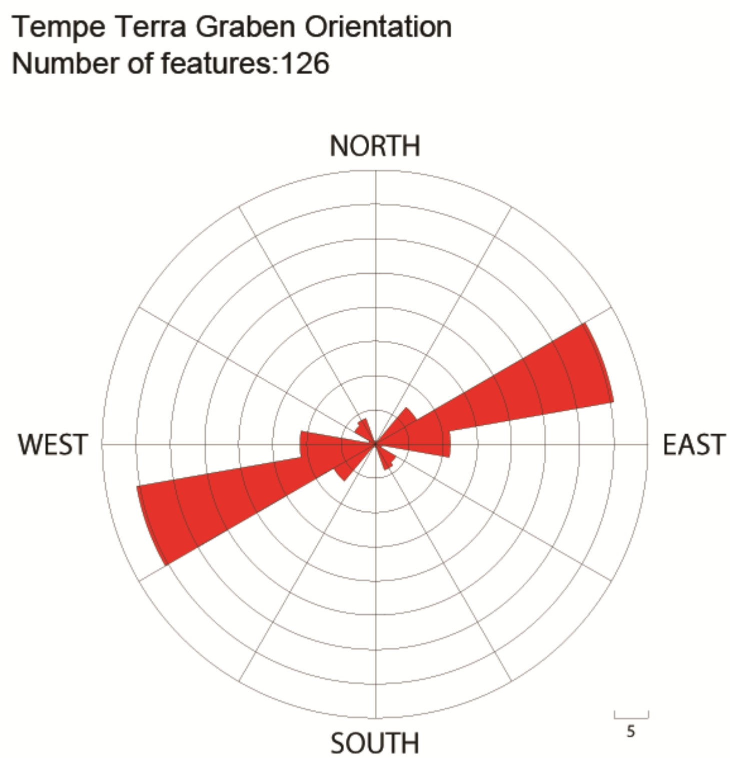

Figure 22. Rose diagram of graben azimuths. NE-SW graben dominate the area with smaller secondary populations with W-E and NW-SE azimuths. The minor populations represent older, more obscured graben.

error of +/- 700 My. Additionally, a volcano is constructed from multiple eruptive episodes and when the entire flank of a volcano is treated as one unit, the derived age is a combination of multiple ages. Some of the shields measured have diameters less than 10 km. Using MOLA data for features this small may introduce unquantifiable error due to the footprint size of the laser. MOLA gridded data was also used, as opposed to single MOLA tracks that may introduce interpolation errors between locations of actual measurement, although most features are large enough that this should not pose any significant problems. As with any work that measures "real world" features as opposed to perfect models, there is no one true diameter, height, or slope for a volcano. To offset this, heights and flank widths were measured four times and an average was used.

Conclusions and Future Work

The TVP is similar to other fields of low shields on Mars, as well as the SRP on Earth. This work further supports that hypothesis and better constrains the period of activity for the TVP. Shield building eruptions have occurred in the TVP for over half of the planet's geologic history, 2.4 Ga to possibly as young as 120 Ma. Morphological trends, such as average flank slope and relief versus age suggest that the TVP magma system has evolved with time, resulting in some combination of lower effusion rates and more viscous magma. The similarities in morphologies of the TVP shields to those in other fields of low shields could indicate that those fields evolved in the same manner. The temporal distribution of the shields suggests that the location of the magma supply and/or the regional stress field associated with Tharsis favored the migration of volcanic activity to the NE, beginning about 800 My. b.p.

Future work should include determining the ages and morphologies of the unstudied shields in the TVP as well as dating the lava plains that embay some of the shields. Higher resolution DTMs generated from HRSC and CTX stereo images should also be used to get higher resolution topography data. A volcanic map was made for this project using tracing paper over the base map. The next step would be to digitize this map using a GIS software such as ArcMap.

REFERENCES

Anderson, R. C., Dohm, J. M., Golombek, M. P., Haldemann, A. F. C., Franklin, B. J., Tanaka, K. L., . . . Peer, B. (2001). Primary centers and secondary concentrations of tectonic activity through time in the western hemisphere of mars. *Journal of Geophysical Research, 106*(E9), 20563-20585. doi:10.1029/2000JE001278

Baird, A. K., Toulmin, P., Clark, B. C., Rose, H. J., Keil, K., Christian, R. P., & Gooding, J. L. (1976). Mineralogic and petrologic implications of viking geochemical results from mars: Interim report. *Science, 194*(4271), 1288-1293. doi:10.1126/science.194.4271.1288

Bandfield, J. L. (2002). Global mineral distributions on mars. *Journal of Geophysical Research - Planets, 107*(E6), 5042. doi:10.1029/2001JE001510

Baptista, A. R., Veronique, N., Ansan, V., Baratoux, D., Lognonné, P., Alves, E. I., . . . Neukum, G. (2008). A swarm of small shield volcanoes on syria planum, mars. *Journal of Geophysical Research - Planets, 113*(E9), E09010. doi:10.1029/2007JE002945

Baratoux, D., Pinet, P., Toplis, M. J., Mangold, N., Greeley, R., & Baptista, A. R. (2009). Shape, rheology and emplacement times of small martian shield volcanoes. *Journal of Volcanology and Geothermal Research, 185*(1), 47-68. doi:10.1016/j.jvolgeores.2009.05.003

Bleacher, J. E., & Greeley, R. (2008). Relating volcano morphometry to the developmental progression of hawaiian shield volcanoes through slope and hypsometric analyses of SRTM data. *Journal of Geophysical Research - Solid Earth, 113*(B9), B09208. doi:10.1029/2006JB004661

Bleacher, J. E., Greeley, R., Williams, D. A., Cave, S. R., & Neukum, G. (2007b). Trends in effusive style at the tharsis montes, mars, and implications for the development of the tharsis province. *Journal of Geophysical Research - Planets, 112*(E9), E09005. doi:10.1029/2006JE002873

Bleacher, J. E., Glaze, L. S., Greeley, R., Hauber, E., Baloga, S. M., Sakimoto, S. E. H., . . . Glotch, T. D. (2009). Spatial and alignment analyses for a field of small volcanic vents south of pavonis mons and implications for the tharsis province, mars. *Journal of Volcanology and Geothermal Research, 185*(1), 96-102. doi:10.1016/j.jvolgeores.2009.04.008

Bleacher, J. E., Greeley, R., Williams, D. A., Werner, S. C., Hauber, E., & Neukum, G. (2007a). Olympus mons, mars: Inferred changes in late amazonian aged effusive activity from lava flow mapping of mars express high resolution stereo camera data. *Journal of Geophysical Research, 112*(E4) doi:10.1029/2006JE002826

Campbell, I. H. & Griffiths, R. W. (1990). Implications of mantle plume structure for the evolution of flood basalts. *Earth and Planetary Science Letters* 99, 79-93.

Carr, M. H., & Greeley, R. (1980). *Volcanic features of hawaii: A basis for comparison with mars*. Washington DC: National Printing Office.

Carr, M. H., Masursky, H., & Saunders, R. S. (1973). A generalized geologic map of mars. *Journal of Geophysical Research, 78*(20), 4031-4036. doi:10.1029/JB078i020p04031

Carr, M. H. (1973). *Volcanism on mars* - AGU. doi:10.1029/JB078i020p04049

Carr, M. H. (1974). Tectonism and volcanism of the tharsis region of mars. *Journal of Geophysical Research, 79*(26), 3943-3949. doi:10.1029/JB079i026p03943

Christensen, P. R., Engle, E., Anwar, S., Dickenshied, S., Noss, D., Gorelick, N., & Weiss-Malik, M. (2009). JMARS - A planetary GIS [Abstract]. *American Geophysical Union, Fall Meeting 2009, Abstract #IN22A-06,*

Christensen, P. R., Jakosky, B. M., Kieffer, H. H., Malin, M. C., McSween Jr, H. Y., Nealson, K., . . . Ravine, M. (2004). The thermal emission imaging system (THEMIS) for the mars 2001 odyssey mission. *Space Science Reviews, 110*(1), 85-130. doi:10.1023/B:SPAC.0000021008.16305.94

Dohm, J. M., Williams, J., Anderson, R. C., Ruiz, J., McGuire, P. C., Komatsu, G., . . . Wheelock, S. J. (2009). New evidence for a magmatic influence on the origin of valles marineris, mars. *Journal of Volcanology and Geothermal Research, 185*(1), 12-27. doi:10.1016/j.jvolgeores.2008.11.029

Francis, P. W., & Wood, C. A. (1982). Absence of silicic volcanism on mars: Implications for crustal composition and volatile abundance. *Journal of Geophysical Research, 87*(B12), 9881-9889. doi:10.1029/JB087iB12p09881

Greeley, R. (1976). Modes of emplacement of basalt terrains and an analysis of mare volcanism in the orientale basin [Abstract]. *Lunar Science Conference, 7th, Houston, Tex., March 15-19, 1976, Volume 3* 2747-2759.

Greeley, R. (1982). THE SNAKE RIVER PLAIN, IDAHO: REPRESENTATIVE OF A NEW CATEGORY OF VOLCANISM. *Journal of Geophysical Research, 87*(B4), 2705-2712. doi:10.1029/JB087iB04p02705

Greeley, R., & Spudis, P. D. (1981). Volcanism on mars. *Reviews of Geophysics, 19*(1), 13. doi:10.1029/RG019i001p00013

Hartmann, W. K., Strom, R. G., Weidenschilling, S. J., Blasius, K. R., Voronow, A., Dence, M. R., . . . Jones, K. L. (1981). *Basaltic volcanism on the terrestrial planets*. New York: Pergamon Press.

Hartmann, W. K. (1971). Martian cratering III: Theory of crater obliteration. *Icarus, 15*(3), 410-428. doi:10.1016/0019-1035(71)90119-9

Hartmann, W. K. (2005). Martian cratering 8: Isochron refinement and the chronology of mars. *Icarus, 174*(2), 294-320. doi:10.1016/j.icarus.2004.11.023

Hartmann, W. K., & Neukum, G. (2001). Cratering chronology and the evolution of mars. *Space Science Reviews, 96*(1), 165-194. doi:10.1023/A:1011945222010

Hauber, E., Broz, P., Jagert, F., Jodlowski, P., & Platz, T. (2011). Very recent and wide-spread basaltic volcanism on mars. *Geophysical Research Letters, 38*(1) doi:10.1029/2011GL047310

Hauber, E., Bleacher, J., Gwinner, K., Williams, D., & Greeley, R. (2009). The topography and morphology of low shields and associated landforms of plains volcanism in the tharsis region of mars. *Journal of Volcanology and Geothermal Research, 185*(1), 69-95. doi:10.1016/j.jvolgeores.2009.04.015

Head, J. W. (2001). Volcanism on mars: New perspectives from MOLA topography. *, GSA Annual Meeting (2001)*(Paper no. 178-0)

Hodges, C. A. (1979). Some lesser volcanic provinces on mars. *NASA Tech. Memo., TM-80339*, 247-249.

Hodges, C. A. (1980a). Tempe-mareotis volcanic province of mars. *NASA Tech Memo, TM-91776*, 181-183.

Hodges, C. A., & Moore, H. J. (1994). *Atlas of volcanic landforms on mars.* (No. 1534). Denver, CO: For sale by U.S. Geological Survey, Map Distribution.

Hughes, S. S., Sakimoto, S. E. H., & Gregg, T. K. P. (2008). A petrogenetic model of plains-style low shield volcanoes on mars-implications for magma production in the tharsis region [Abstract]. *39th Lunar and Planetary Science Conference, (Lunar and Planetary Science XXXIX), LPI Contribution No. 1391* 1619.

Ivanov, B. A. (2001). Mars/Moon cratering rate ratio estimates. *Space Science Reviews, 96*(1), 87-104. doi:10.1023/A:1011941121102

Kneissl, T., van Gasselt, S., & Neukum, G. (2011). Map-projection-independent crater size-frequency determination in GIS environments—New software tool for ArcGIS. *Planetary and Space Science, 59*(11–12), 1243-1254. doi:10.1016/j.pss.2010.03.015

Lanz, J. K., & Saric, M. B. (2009). Cone fields in SW elysium planitia: Hydrothermal venting on mars? *Journal of Geophysical Research - Planets, 114*(E2), E02008. doi:10.1029/2008JE003209

Malin, M. C., Bell III, J. F., Cantor, B. A., Caplinger, M. A., Calvin, W. M., Clancy, R. T., . . . Wolff, M. J. (2007). Context camera investigation on board the mars reconnaissance orbiter. *Journal of Geophysical Research - Planets, 112*(E5), E05S04. doi:10.1029/2006JE002808

Malin, M. C., Carr, M. H., Danielson, G. E., Davies, M. E., Hartmann, W. K., Ingersoll, A. P., . . . Warren, J. L. (1998). Early views of the martian surface from the mars orbiter camera of mars global surveyor. *Science, 279*(5357), 1681-1685. doi:10.1126/science.279.5357.1681

Malin, M., & Edgett, K. (2001). Mars global surveyor mars orbiter camera: Interplanetary cruise through primary mission. *Journal of Geophysical Research - Planets, 106*(E10), 23429-23570.

McEwen, A. S., Eliason, E. M., Bergstrom, J. W., Bridges, N. T., Hansen, C. J., Delamere, W. A., . . . Catherine M. Weitz. (2007). Mars reconnaissance orbiter's high resolution imaging science experiment (HiRISE). *Journal of Geophysical Research - Planets, 112*(E5), E05S02. doi:10.1029/2005JE002605

McEwen, A. S., Preblich, B. S., Turtle, E. P., Artemieva, N. A., Golombek, M. P., Hurst, M., . . . Christensen, P. R. (2005). The rayed crater zunil and interpretations of small impact craters on mars. *Icarus, 176*(2), 351-381. doi:10.1016/j.icarus.2005.02.009

McSween, H. Y., Jr. (1994). What we have learned about mars from SNC meteorites. *Meteoritics, 29*(6), 757-779.

McSween, H. Y.,Jr. (1984). SNC meteorites: Are they martian rocks? *Geology, 12*(1), 3. doi:10.1130/0091-7613

Michael, G. G., & Neukum, G. (2010). Planetary surface dating from crater size–frequency distribution measurements: Partial resurfacing events and statistical age uncertainty. *Earth and Planetary Science Letters, 294*(3–4), 223-229. doi:10.1016/j.epsl.2009.12.041

Moore, H. J. (2001). *Geologic map of the tempe-mareotis region of mars: U.S. geological survey geologic investigations series I–2727* USGS.

Mouginis-Mark, P. J., Wilson, L., & Head, J. W. (1982). Explosive volcanism on hecates tholus, mars: Investigation of eruption conditions. *Journal of Geophysical Research, 87*(B12), 9890-9904. doi:10.1029/JB087iB12p09890

Neesemann, A., van Gasselt, S., Hauber, E., & Neukum, G. (2010). Detailed mapping of tempe terra, mars: Geology, tectonic and stratigraphy of refined units [Abstract]. *Geophysical Research Abstracts, Vol. 12, EGU2010-6837-1*

Neukum, G., & Jaumann, R. (2004a). HRSC: The High Resolution Stereo Camera of Mars Express [Abstract]. *In: Mars Express: The Scientific Payload. Ed. by Andrew Wilson, Scientific Coordination: Agustin Chicarro. ESA SP-1240, Noordwijk, Netherlands: ESA Publications Division, ISBN 92-9092-556-6,* 17-35.

Neukum, G., & Hiller, K. (1981). Martian ages. *Journal of Geophysical Research, 86*(B4), 3097-3121. doi:10.1029/JB086iB04p03097

Pike, R. J. (1978). Volcanoes on the inner planets - some preliminary comparisons of gross topography. *Lunar and Planetary Science Conference, 9th, Houston, Tex., March 13-17, 1978, 3*, 3239-3273.

Platz, T., & Michael, G. (2011). Eruption history of the elysium volcanic province, mars. *Earth and Planetary Science Letters, 312*(1-2), 140. doi:10.1016/j.epsl.2011.10.001

Plescia, J. B. (1980). The tempe volcanic province: An analog to the eastern snake river plains? [Abstract]. *NASA Tech Memo, TM-91776* 189-191.

Plescia, J. B. (1981). The tempe volcanic province of mars and comparisons with the snake river plains of idaho. *Icarus, 45*(3), 586-601. doi:10.1016/0019-1035(81)90024-5

Plescia, J. B., & Golombek, M. P. (1986). Origin of planetary wrinkle ridges based on the study of terrestrial analogs. Geol. Soc. Amer. Bull. 97, 1289–1299. doi:10.1130/0016-7606(1986)97<1289:OOPWRB>2.0.CO;2

Robinson, M. S., Mouginis-Mark, P. J., Zimbelman, J. R., Wu, S. S. C., Ablin, K. K., & Howington-Kraus, A. E. (1993). Chronology, eruption duration, and atmospheric contribution of the martian volcano apollinaris patera. *Icarus, 104*(2), 301-323. doi:10.1006/icar.1993.1103

Ruff, S. W., Christensen, P. R., Blaney, D. L., Farrand, W. H., Johnson, J. R., Michalski, J. R., . . . Squyres, S. W. (2006). The rocks of gusev crater as viewed by the mini-TES instrument. *Journal of Geophysical Research - Planets, 111*(E12), E12S18. doi:10.1029/2006JE002747

Ryan, A. J., & Christensen, P. R. (2012). Coils and polygonal crust in the athabasca valles region, mars, as evidence for a volcanic history. *Science, 336*(6080), 449-452. doi:10.1126/science.1219437

Sakimoto, S. E. H. (2008). Martian small volcanic shields and shield fields [Abstract]. *39th Lunar and Planetary Science Conference, (Lunar and Planetary Science XXXIX), Held March 10-14, 2008 in League City, Texas. LPI Contribution no. 1391., p.1658,*

Sakimoto, S. E. H., Gregg, T. K. P., Hughes, S. S., & Chadwick, J. (2003). Re-assessing plains-style volcanism on mars [Abstract]. *Sixth International Conference on Mars, July 20-25 2003, Pasadena, California, abstract no.3197*

Self S, Thordarson T & Keszthelyi L (1997) Emplacement of continental flood basalt lava flows. *In: Mahoney JJ & Coffin MF (eds) Large Igneous Provinces: Continental, Oceanic, and Planetary Flood Volcanism. Geophys. Monogr*. 100, 381-410. doi:10.1029/GM100p0381

Scott, D. H., & Carr, M. H. (1978). *Geologic map of mars. U. S. geological survey. map I-1083. scale 1:25,000,000* USGS.

Scott, D. H., & Dohm, J. M. (1990). Faults and ridges - historical development in tempe-terra and ulysses-patera regions of mars. *Proceedings of the Lunar and Planetary Science Conference, 20*, 503-513.

Scott, D. H. (1982). Volcanoes and volcanic provinces: Martian western hemisphere. *Journal of Geophysical Research, 87*(B12), 9839-9851. doi:10.1029/JB087iB12p09839

Smith, D. E., Neumann, G., Arvidson, R. E., Guinness, E. A., & Slavney, S. (2003). *Mars global surveyor laser altimeter mission experiment gridded data record*

Smith, D. E., Zuber, M. T., Frey, H. V., Garvin, J. B., Head, J. W., Muhleman, D. O., . . . Sun, X. (2001b). Mars orbiter laser altimeter: Experiment summary after the first year of global mapping of mars. *Journal of Geophysical Research, 106*(E10), 23689-23722. doi:10.1029/2000JE001364

Steinberger, B., Werner, S. C., & Torsvik, T. H. (2010). Deep versus shallow origin of gravity anomalies, topography and volcanism on earth, venus and mars. *Icarus, 207*(2), 564-577. doi:10.1016/j.icarus.2009.12.025

Torson, J. M., & Becker, K. J. (1997). ISIS - A software architecture for processing planetary images [Abstract]. *LPSC XXVIII,* 1443-1444.

Walker, G. (1971). *Compound and simple lava flows and flood basalts* Springer Berlin / Heidelberg. doi:10.1007/BF02596829

Watters, T. R. (1988). Wrinkle ridge assemblages on the terrestrial planets. *Journal of Geophysical Research, 93*(B9), 10236-10254. doi:10.1029/JB093iB09p10236

Werner, S. C. (2009). The global martian volcanic evolutionary history. *Icarus, 201*(1), 44-68. doi:10.1016/j.icarus.2008.12.019

White, R., & McKenzie, D. (1989). Magmatism at rift zones: The generation of volcanic continental margins and flood basalts. *Journal of Geophysical Research, 94*(B6), 7685-7729. doi:10.1029/JB094iB06p07685

Wilhelms, D. E. (1990). *Planetary mapping edited by ronald greeley and raymond M. batson*. Cambridge: Cambridge University Press.

Williams, D. A., Greeley, R., Fergason, R. L., Kuzmin, R., McCord, T. B., Combe, J., . . . Poulet, F. (2009). The circum-hellas volcanic province, mars: Overview. *Planetary and Space Science, 57*(8-9), 895-916. doi:10.1016/j.pss.2008.08.010

Wilson, L., & Head III, J. W. (2002). Tharsis-radial graben systems as the surface manifestation of plume-related dike intrusion complexes: Models and implications. *Journal of Geophysical Research - Planets, 107*(E8), 5057. doi:10.1029/2001JE001593

Wilson, L., & Head, J. W. (1994). Mars – Review and analysis of volcanic eruption theory and relationships to observed landforms. *Reviews of Geophysics, 32*(3), 221-263.

Wise, D. U. (1979). *Geologic map of the arcadia quadrangle of mars map I-1154 (MC-3)* USGS.

Wong, M. P., Sakimoto, S. E. H., & Garvin, J. B. (2001). MOLA topography of small volcanoes in tempe terra and ceraunius fossae, mars: Implications for eruptive styles. *32nd Annual Lunar and Planetary Science Conference, March 12-16, 2001, Houston, Texas, abstract no.1563*

Zuber, M. T., Smith, D. E., Solomon, S. C., Muhleman, D. O., Head, J. W., Garvin, J. B., . . . Bufton, J. L. (1992). *The mars observer laser altimeter investigation* - AGU. doi:10.1029/92JE00341